Journal of Medicinal Chemistry

Article

pubs.acs.org/jmc

Discovery of a Small-Molecule Degrader of Bromodomain and Extra-Terminal (BET) Proteins with Picomolar Cellular Potencies and Capable of Achieving Tumor Regression

Bing Zhou,[†,‡,▽] Jiantao Hu,[†,‡,▽] Fuming Xu,[†,‡,▽] Zhuo Chen,[†,‡,▽] Longchuan Bai,[†,‡,▽] Ester Fernandez-Salas,[†,§,▽] Mei Lin,[†,‡,▽] Liu Liu,[†,‡] Chao-Yie Yang,[†,‡] Yujun Zhao,[†,‡] Donna McEachern,[†,‡] Sally Przybranowski,[†,‡] Bo Wen,[†,∥] Duxin Sun,[†,∥] and Shaomeng Wang*[,†,‡,⊥,#]

[†]University of Michigan Comprehensive Cancer Center, and Departments of [‡]Internal Medicine, [§]Pathology, [∥]Pharmaceutical Sciences, [⊥]Medicinal Chemistry, and [#]Pharmacology, University of Michigan, Ann Arbor, Michigan 48109, United States

Supporting Information

ABSTRACT: The bromodomain and extra-terminal (BET) family proteins, consisting of BRD2, BRD3, BRD4, and testis-specific BRDT members, are epigenetic "readers" and play a key role in the regulation of gene transcription. BET proteins are considered to be attractive therapeutic targets for cancer and other human diseases. Recently, heterobifunctional small-molecule BET degraders have been designed based upon the proteolysis targeting chimera (PROTAC) concept to induce BET protein degradation. Herein, we present our design, synthesis, and evaluation of a new class of PROTAC BET degraders. One of the most promising compounds, **23**, effectively degrades BRD4 protein at concentrations as low as 30 pM in the RS4;11 leukemia cell line, achieves an IC_{50} value of 51 pM in inhibition of RS4;11 cell growth and induces rapid tumor regression in vivo against RS4;11 xenograft tumors. These data establish that compound **23** (BETd-260/ZBC260) is a highly potent and efficacious BET degrader.

PROTAC BET Degrader **23**

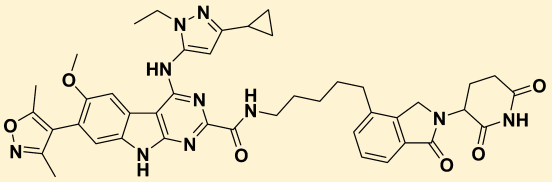

IC_{50} = 51 pM in Cell Growth Inhibition in RS4;11 Cells

INTRODUCTION

Bromodomain-containing proteins are epigenetic "readers". By binding to acetylated lysine residues on the histone tails, bromodomain-containing proteins play a key role in regulation of gene transcription.[1] Among bromodomain-containing proteins, the bromodomain and extra-terminal domain (BET) family of proteins, consisting of BRD2, BRD3, BRD4, and testis-specific BRDT members, have emerged as exciting new therapeutic targets for cancer and other human diseases.[2−6] The discovery of **1** ((+)-JQ-1) as the first potent and selective BET inhibitor (Figure 1) has greatly promoted investigations of BET proteins as new therapeutic targets in human cancers and other diseases.[7] Several BET inhibitors such as **2** (OTX015) and **3** (I-BET762) (Figure 1) have been advanced into clinical development.[8−13] Recently, preliminary clinical data have provided an important clinical proof-of-concept that BET inhibition has therapeutic potential for the treatment of certain forms of human cancer, including NUT (nuclear protein in testis) midline carcinoma, multiple myeloma, and acute myeloid leukemia (AML).[7,10,11,14] Preclinical studies have also suggested that BET inhibitors may have therapeutic potential for the treatment of other human cancers, as well as other human diseases and conditions.[15−19]

Small-molecule BET inhibitors are designed to bind the BET bromodomains and to block the interaction of BET proteins with acetylated lysine residues on histone tails to regulate gene transcription. In addition to small-molecule BET inhibitors, a new approach has recently been developed to target BET proteins for degradation based upon the proteolysis targeting chimera (PROTAC) concept.[20] In this approach, a hetero-bifunctional (chimeric) molecule is designed to contain a BET inhibitor, which binds to BET proteins, another small-molecule ligand, which binds to an E3 ubiquitin ligase complex, and a linker to tether these two ligands together.[21,22] A number of BET degraders have been reported, including **4** (dBET1),[23] **5** (ARV-771),[24] **6** (ARV-825),[25] and MZ1[26] (Figure 1). Compounds **4** and **6** were designed using **1** or **2**, two closely related BET inhibitors, and thalidomide, which is a ligand for cereblon, a component of the Cullin4A ubiquitin ligase complex.[23,25] In comparison, BET degrader **5** was designed using **1** for the BET inhibitor portion and a ligand for the von Hippel−Lindau E3 ubiquitin ligase.[24] These BET degraders have been shown to efficiently induce BET protein degradation and to be more potent in inhibition of cancer cell growth and in induction of apoptosis than their corresponding BET inhibitors. Compound **4** is more effective in inhibition of tumor growth in

Special Issue: Inducing Protein Degradation as a Therapeutic Strategy

Received: December 11, 2016
Published: March 24, 2017

DOI: 10.1021/acs.jmedchem.6b01816
J. Med. Chem. 2018, 61, 462−481

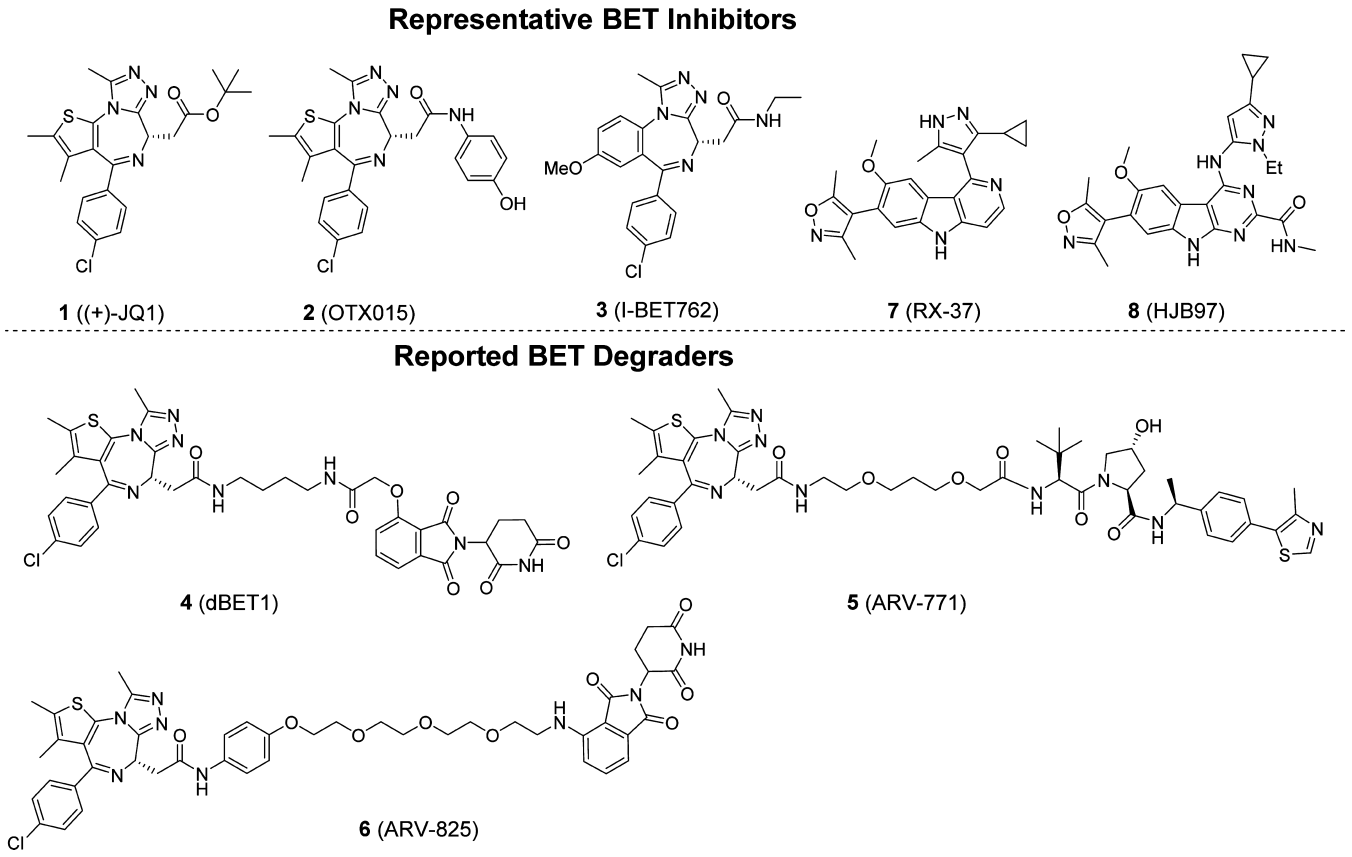

Figure 1. Chemical structures of representative BET inhibitors **1**, **2**, **3**, **7**, **8** and three representative previously reported BET degraders **4**, **5**, and **6**.

Table 1. Binding Affinities of BET Inhibitors

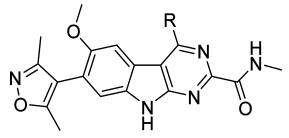

Compound	R	Binding Affinities (IC_{50}/K_i, nM)[a]					
		BRD2		BRD3		BRD4	
		BD1	BD2	BD1	BD2	BD1	BD2
1		36.1±5.1/ 13.2±4.5	53.3±8.6/ 12.5±2.7	39.1±6.5/ 6.6±1.2	56.7±10.5/ 8.9±1.6	46.7±4.4/ 14.9±2.6	42.2±9.1/ 12.0±3.5
2		33.3±1.6/ 16.6±1.0	24.8±1.0/ 5.4±0.2	38.5±0.8/ 10.7±1.0	21.0±2.7/ 4.0±0.6	25.5±1.0/ 10.9±0.6	16.6±1.1/ 6.0±0.3
8	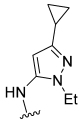	3.1±0.7/ 0.9±0.2	3.9±0.5/ 0.27±0.09	6.6±0.2/ 0.18±0.01	1.9±0.4/ 0.21±0.03	7.0±0.6/ 0.5±0.2	7.0±0.1/ 1.0±0.1
28	H	218±6/ 101±5	224±6/ 57.3±3.4	294±37/ 82.1±7.4	189±21/ 42.4±4.6	484±58/ 152±11	630±88/ 205±28

[a] IC_{50} values were obtained from three separate experiments.

vivo than **1** in an acute leukemia model in mice,[23] and compound **5** achieves effective inhibition of tumor growth in a castration-resistance prostate cancer xenograft model in mice.[24] Collectively, these studies provide evidence that small-molecule

DOI: 10.1021/acs.jmedchem.6b01816
J. Med. Chem. 2018, 61, 462−481

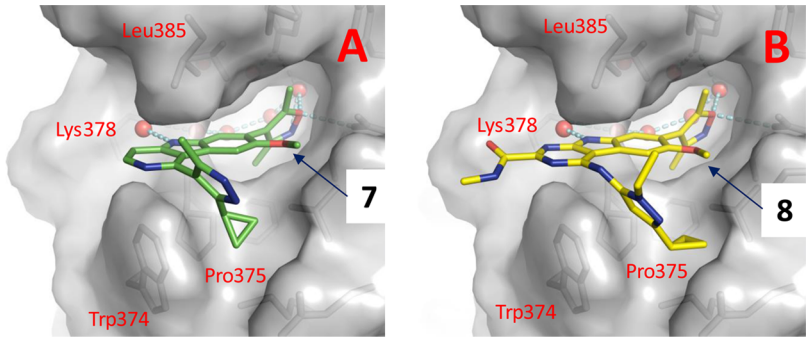

Figure 2. (A) Cocrystal structure of BRD4 BD2 complexed with **7** (green, PDB code 4Z93). (B) Modeled structure of BRD4 BD2 complexed with **8** (yellow). Water molecules are shown as red spheres. Hydrogen bonds are depicted in dashed lines. Residues in BRD4 BD2 close to the proposed linkage site of **8** are labeled in red.

Table 2. Optimization of Linker Length and Composition

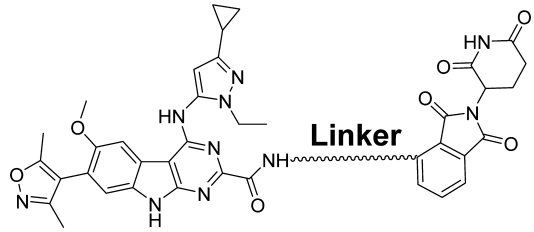

Compound	Linker	IC_{50} (nM) in cell growth inhibition[a]	
		RS4;11	MOLM-13
4	-	78.8 ± 11.7	657 ± 326
6	-	3.3 ± 0.7	18.2 ± 4.0
8	-	24.1 ± 5.3	25.6 ± 1.9
9	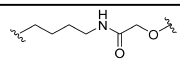	4.3 ± 3.1	45.5 ± 14.1
10	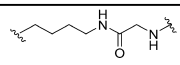	2.5 ± 1.0	19.9 ± 2.5
11	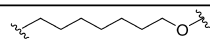	0.48 ± 0.03	3.9 ± 0.7
12	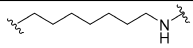	0.20 ± 0.02	1.2 ± 0.2
13	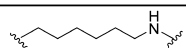	0.63 ± 0.13	3.7 ± 0.1
14	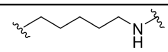	0.14 ± 0.06	2.1 ± 1.1
15	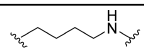	0.45 ± 0.21	5.0 ± 1.3
16	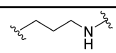	2.4 ± 1.0	9.5 ± 2.3
17	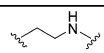	4.8 ± 2.6	68.7 ± 19.7

[a] IC_{50} values were obtained from three independent experiments.

degraders of BET proteins may have a promising therapeutic potential for the treatment of human cancers and potentially other diseases and conditions.

Recently, our laboratory reported the discovery of azacarbazoles as a new class of potent and selective BET bromodomain inhibitors.[27] In the present study, we report the discovery of a new class of small-molecule BET degraders designed based upon our azacarbazole-based BET inhibitors and thalidomide/lenalidomide as ligands for cereblon/Cullin4A. Through extensive optimization of the linker region, we have obtained a series of highly potent BET degraders. Among these, compound **23** (BETd-260) is capable of inducing degradation of BRD2, BRD3, and BRD4 proteins at 30−100 pM in the RS4;11 leukemia cells. Compound **23** achieves an IC_{50} value of 51 pM in inhibition of the RS4;11 cell growth and induces rapid tumor regression of the RS4;11 xenograft tumors with no signs of toxicity in mice. Compound **23** is a highly potent and efficacious BET degrader and warrants extensive

DOI: 10.1021/acs.jmedchem.6b01816
J. Med. Chem. 2018, 61, 462−481

evaluation for the treatment of human cancers and other diseases.

RESULTS AND DISCUSSION

Starting from our previously reported BET inhibitor 7[27] (Figure 1), we performed further optimization for this class of BET inhibitors and identified **8** (HJB97) as a high-affinity BET inhibitor. In our FP-based competitive binding assays, **8** binds to BRD2, BRD3, and BRD4 with high affinities (K_i < 1 nM) and is >10 times more potent than **1** or **2** (Table 1). Compound **8** also potently inhibits cell growth in RS4;11 and MOLM-13 acute leukemia cell lines, which are known to be sensitive to BET inhibitors. Hence, compound **8** is a potent BET inhibitor and was employed in our design of BET degraders.

Upon the basis of the cocrystal structure of BRD4 BD2 complexed with **7** (PDB code 4Z93), we modeled the structure of BRD4 BD2 complexed with **8** (Figure 2). Our modeled structure showed that the 2-carboxamide group attached to the [6,5,6] tricyclic system in **8** is exposed to solvent, making it a suitable site for tethering to thalidomide/lenalidomide for the design of potential PROTAC degraders of BET proteins (Figure 2). Accordingly, we designed and synthesized **9** as a potential BET degrader using **8** for the BET inhibitor portion, thalidomide as the cereblon ligand, and the same linker that was used in **4**. In a cell growth assay, the BET degrader **9** has an IC_{50} value of 4.3 nM in the RS4;11 acute leukemia cell line and is 6 times more potent than the corresponding BET inhibitor **8** (Table 2). Western blotting analysis showed that **9**, at concentrations as low as 3−10 nM, is effective in decreasing the level of BRD2, BRD3, and BRD4 proteins in the RS4;11 cells whereas the BET inhibitor **8** at both 100 and 300 nM fails to decrease the level of BRD2−4 proteins (Figure 3). Two

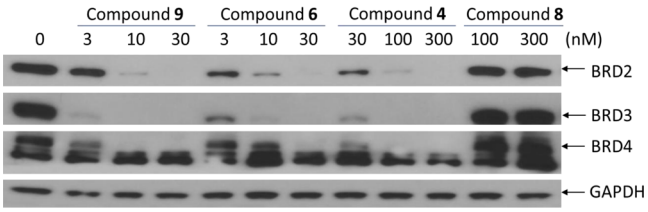

Figure 3. Western blotting analysis of BRD2, BRD3, and BRD4 proteins in RS4;11 cells treated with BET degraders **4**, **6**, and **9** and BET inhibitor **8**. RS4;11 cells were treated for 3 h with each individual compound at indicated concentrations, and proteins were probed by specific antibodies. GAPDH was used as the loading control.

previously reported BET degraders, **4** and **6**, also effectively decrease the level of BRD2−4 proteins in the RS4;11 cell line (Figure 3). Consistent with its testis-specific expression, BRDT protein was not detected in the RS4;11 cells. We concluded that **9** is a promising BET degrader for further optimization.

We next explored the length and the composition of the linker in **9**. Replacing the oxygen atom in **9** with an amino group resulted in **10**, whose cell growth inhibitory activity is 2 times better than that of **9**. Conversion of the amide group (-CO-NH-) in **9** to an ethylene group (-CH_2-CH_2-) generated **11**, which has an IC_{50} value of 0.48 nM in inhibition of cell growth in the RS4;11 cell line and is thus 10 times more potent than **9**. Similar conversion of the amide group in **10** to an ethylene group yielded **12** which, with an IC_{50} value of 0.20 nM in inhibition of RS4;11 cell growth, is 10 times more potent than **10**. These data demonstrate that both the length and the composition of the linker have a considerable influence on the cellular potencies of the resulting BET degraders.

We next sought to determine the optimal linker length in **12** for cellular potencies by shortening the linker by one methylene group progressively, which resulted in compounds **13**−**17** (Table 2). Compound **13** with a linker one methylene group shorter than that in **12** is 3 times less potent than **12**. However, compound **14** with two methylene groups shorter than **12** in the linker achieves an IC_{50} value of 0.14 nM in inhibition of RS4;11 cell growth and is slightly more potent than **12**. Shortening the linker in **14** by one additional methylene group resulted in **15**, which is ∼3 times less potent than **14** in inhibition of RS4;11 cell growth, and further shortening the linker in **15** by one methylene or ethylene group yielded **16** or **17**, respectively, which is 5 and 10 times less potent than **15**, respectively, in inhibition of RS4;11 cell growth. These data demonstrate that for achieving the most potent cell growth inhibition activity, an optimal linker length should comprise -$(CH_2)_{4-7}$NH- in these BET degraders, as is shown in compounds **12**−**15**. When the linker becomes too short as in, for examples, compounds **16** and **17**, the cellular potency is greatly decreased.

To investigate whether the SAR results obtained in the RS4;11 cell line are valid in a different cell line, we evaluated this series of compounds together with **4** and **6** as control compounds for their cell growth inhibitory activity in the MOLM-13 leukemia cell line, which harbors a mixed lineage leukemia protein 1 (MLL1) fusion gene and is also responsive to BET inhibitors in our previous study.[27] The data obtained are summarized in Table 2. In general, the IC_{50} values obtained for all these BET degraders in the MOLM-13 cell line are 5−10 times higher than those obtained in the RS4;11 cell line. Compounds **6** and **4** have IC_{50} values of 18.2 nM and 657 nM, respectively, in inhibition of MOLM-13 cell growth and are 5.5 and 8.3 times less potent than those in the RS4;11 cell line. We obtained a very similar SAR result for BET degraders **9**−**17** in the MOLM-13 cell line when compared to that in the RS4;11 cell line. Compounds **12** and **14** are two of the most potent BET degraders in this series with IC_{50} values of 1.2 nM and 2.1 nM, respectively, in inhibition of MOLM-13 cell growth.

Having determined the optimal linker length, we next performed further modifications of the linker composition in compound **14** (Table 3). Replacement of the NH group in **14** with a methylene group yielded **18**, which with an IC_{50} value of 0.17 nM in inhibition of RS4;11 cell growth is as potent as **14**. Replacement of one methylene group in **18** with an oxygen atom generated **19**, which has an IC_{50} value of 0.42 nM in inhibition of RS4;11 cell growth and is 2 times less potent than **18**. Shortening the linker in **18** by one methylene group resulted in **20** which, with an IC_{50} value of 0.14 nM in inhibition of RS4;11 cell growth, is equipotent to **14**. Thus, modifications of the linker compositions identified compounds **18** and **20** as two very potent BET degraders with subnanomolar IC_{50} values in inhibition of RS4;11 cell growth.

In all of the above synthesized compounds, we employed thalidomide as the ligand for cereblon. Lenalidomide has been developed as a second generation thalidomide analogue for the treatment of multiple myeloma and myelodysplastic syndromes.[28] Although thalidomide and lenalidomide have similar binding affinities to cereblon,[29] they may have different cell permeability and/or pharmacokinetic profiles, and thus we investigated the effect of replacing thalidomide with lenalido-

DOI: 10.1021/acs.jmedchem.6b01816
J. Med. Chem. 2018, 61, 462−481

Table 3. Further Optimization of the Linker and Phthalimide Moiety

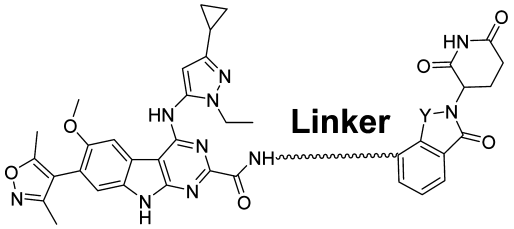

Compound	Linker	Y	IC_{50} (nM) in cell growth inhibition[a]	
			RS4;11	MOLM-13
14	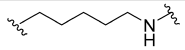	CO	0.14 ± 0.06	2.1 ± 1.1
18	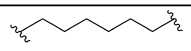	CO	0.17 ± 0.07	2.5 ± 0.7
19	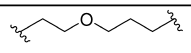	CO	0.42 ± 0.25	5.9 ± 2.8
20	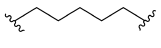	CO	0.14 ± 0.04	2.1 ± 1.0
21	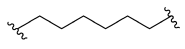	CH_2	0.037 ± 0.023	1.0 ± 0.5
22	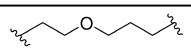	CH_2	0.90 ± 0.15	5.4 ± 1.8
23	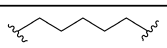	CH_2	0.051 ± 0.018	2.2 ± 0.2
24	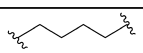	CH_2	0.98 ± 0.14	13.7 ± 2.7
25	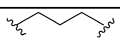	CH_2	9.6 ± 2.2	72.3 ± 10.6

[a]IC_{50} values were obtained from three independent experiments.

Table 4. Investigation of the Effect of BET Protein and Cereblon Binding on Cellular Potencies of BET Degraders

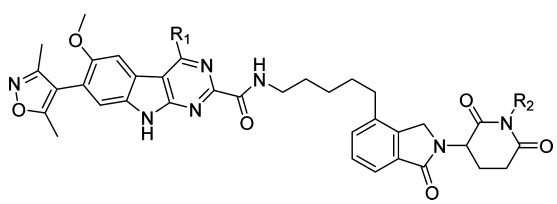

Compound	R1	R2	IC_{50} (nM) in cell growth inhibition[a]	
			RS4;11	MOLM-13
23		H	0.051 ± 0.018	2.2 ± 0.2
26		Me	35.1 ± 12.7	83.4 ± 5.1
27	H	H	>1000	>1000

[a]IC_{50} values were obtained from three independent experiments.

mide in three potent BET degraders **18**, **19**, and **20**. This effort resulted in **21**, **22**, and **23**, which achieve IC_{50} values of 0.037 nM, 0.90 nM, and 0.051 nM, respectively, in inhibition of RS4;11 cell growth. Hence, **21** and **23** are 2−3 times more potent than **18** and **20**. Interestingly, in contrast to **21** and **23**, compound **22** has an IC_{50} value of 0.9 nM in inhibition of RS4;11 cell growth and is thus 2 times less potent than **19**. To further confirm the significance of the linker length, we synthesized compounds **24** and **25** with one methylene or ethylene group shorter than that in **23**. Compounds **24** and **25** have IC_{50} values of 0.98 nM and 9.6 nM in inhibition of RS4;11

DOI: 10.1021/acs.jmedchem.6b01816
J. Med. Chem. 2018, 61, 462−481

cell growth, respectively, and are therefore 19 and 188 times less potent than **23**.

To further investigate the mechanism of action for this class of BET degraders, we have designed two control compounds based upon **23**. It has been shown that installation of a methyl group on the amino group in the lenalidomide moiety blocks the binding of thalidomide analogues to cereblon.[25,29] Accordingly, we installed a methyl group on the amino group in the lenalidomide moiety, which resulted in **26** (Table 4). Compound **26** has an IC_{50} value of 35.1 nM in inhibition of RS4;11 cell growth and is therefore >600 times less potent than **23**, but the IC_{50} is similar to that obtained for the BET inhibitor **8**. Furthermore, **26** fails to induce degradation of BRD2, BRD3, and BRD4 proteins in the RS4;11 cell line, indicating that it inhibits cell growth by acting not as a BET degrader but as a BET inhibitor (Figure S1 in Supporting Information). We synthesized compound **27** based upon a less potent BET inhibitor **28**, which binds to BRD2, BRD3, and BRD4 proteins with affinities of >100 times less potent than that of **8** (Table 1). Compound **27** has an IC_{50} value of >1000 nM and is thus >10 000 and >400 times less potent than **23** in RS4;11 and MOLM13 cell growth inhibition assays, respectively (Table 4). These data indicate that in order to achieve potent cell growth inhibition, a BET degrader must be able to bind to both BET proteins and to the ubiquitin ligase complex, which is consistent with their PROTAC design and the expected mechanism of action.

We examined the ability of four representative BET degraders (**21** and **23**–**25**) to induce BET degradation in the RS4;11 cell line, and the data are shown in Figure 4. All these

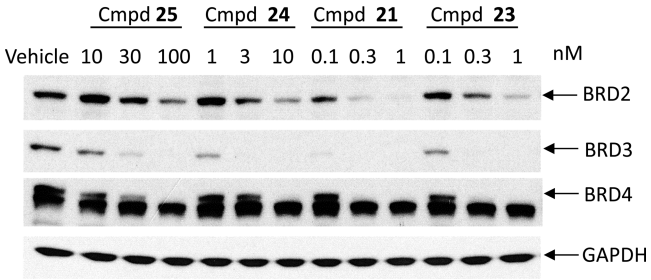

Figure 4. Western blotting analysis of BRD2, BRD3, and BRD4 proteins in RS4;11 cells treated with compounds **21** and **23**–**25**. RS4;11 cells were treated for 3 h with individual compounds at indicated concentrations, and proteins were probed by specific antibodies. GAPDH was used as the loading control.

four compounds can effectively and potently induce degradation of BET proteins in a dose-dependent manner after a 3 h treatment, and their potencies in reducing the levels of BRD2–4 proteins correlate well with their cellular potencies in inhibition of cell growth in the RS4;11 cell line. At concentrations as low as 10 nM, **25** effectively decreases the level of BRD3 and BRD4 proteins but is less potent and effective in decreasing in the level of BRD2 protein. Compound **24** is very effective in reducing the level of BRD2 and BRD4 at concentrations as low as 3 nM and the level of BRD3 at 1 nM. The two most potent BET degraders, **21** and **23**, are highly effective in decreasing the level of BRD2 and BRD4 proteins at concentrations as low as 0.3 nM and decreasing the level of BRD3 at 0.1 nM with a 3 h treatment. Therefore, **21** and **23** are extremely potent degraders of BET proteins.

We further investigated the potency of compound **23** in inducing BET protein degradation in the RS4;11 cells with a 24 h treatment, with compound **8** included as a control (Figure 5).

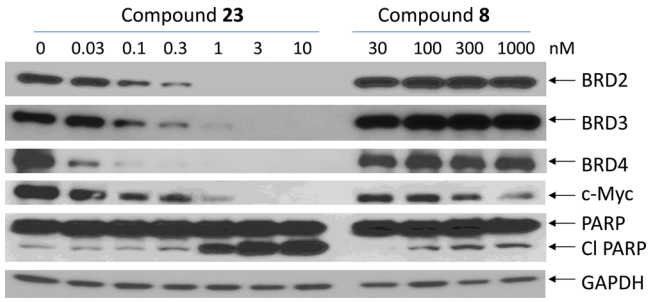

Figure 5. Western blotting analysis of BRD2, BRD3, and BRD4 proteins, as well as c-Myc and PARP in RS4;11 cells treated with BET degrader **23** and BET inhibitor **8**. RS4;11 cells were treated for 24 h with individual compounds at indicated concentrations, and proteins were probed by specific antibodies. GAPDH was used as the loading control.

Compound **23** is capable of effectively reducing the level of BRD2 and BRD3 proteins at concentrations as low as 0.1 nM and the level of BRD4 protein at a concentration of 0.03 nM. In comparison, the BET inhibitor **8** has no effect on the level of BRD2–4 proteins at all concentrations tested (30–1000 nM).

We examined the effects of the BET degrader **23** and the BET inhibitor **8** in the RS4;11 cell line on the level of c-Myc (Figure 5), a protein known to be down-regulated by both BET inhibitors and degraders.[25,30] Consistent with its extremely high potency in inducing BET protein degradation, **23** effectively down-regulates the level of c-Myc at concentrations as low as 0.1 nM. In comparison, the BET inhibitor **8** can also effectively down-regulate the level of c-Myc but at concentrations of 300–1000 nM in the RS4;11 cell line. Hence, the BET degrader **23** is >1000 times more potent than the BET inhibitor **8** in down-regulation of c-Myc protein in the RS4;11 cell line.

The mechanism of action of BET protein degradation by **23** was further investigated (Figure 6). Addition of the BET inhibitor **8** effectively blocks the degradation of BRD2, BRD3, and BRD4 proteins induced by **23** (Figure 6A), further confirming that the degradation of BET proteins by **23** requires its binding to BET proteins. Similarly, addition of lenalidomide also effectively blocks the degradation induced by **23** for all three BET proteins (Figure 6B), clearly indicating that degradation of BET proteins by **23** is cereblon-dependent. The proteasome inhibitor MG-132 and the NEDD8-activating enzyme (NAE) inhibitor MLN4924 also completely block the degradation of BET proteins by **23** (Figure 6C), indicating that BET protein degradation by **23** depends upon proteasome and NAE. These mechanistic data constitute clear evidence that **23** is a bona fide and highly potent BET degrader.

We employed flow cytometry analysis to investigate the ability of the BET degrader **23** and the BET inhibitor **8** to induce cell cycle arrest and apoptosis in the RS4;11 and MOLM-13 cell lines (Figure 7). Both compounds were found to effectively induce cell cycle arrest in a dose-dependent manner in both cell lines, but they have very different potencies. While the BET inhibitor **8** is effective at 30 nM in the RS4;11 cell line in inducing cell cycle arrest, the BET degrader **23** has a strong effect at concentrations as low as 0.3 nM. In the MOLM-13 cell line, **8** is effective at 30–100 nM in

DOI: 10.1021/acs.jmedchem.6b01816
J. Med. Chem. 2018, 61, 462–481

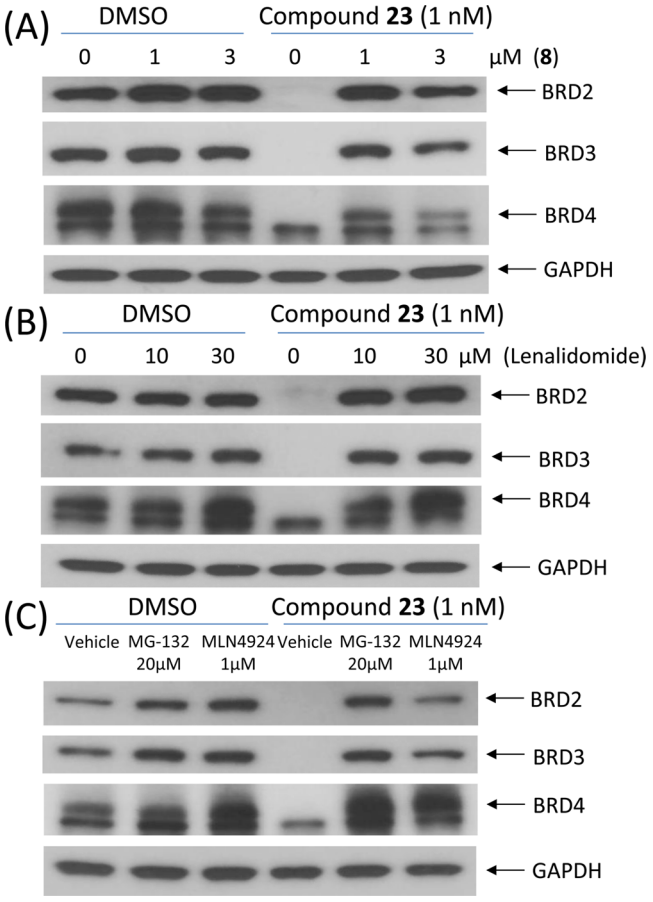

Figure 6. Western blotting analysis of BRD2, BRD3, and BRD4 proteins after a 2 h pretreatment with **8** (A), lenalidomide (B), or a proteasome inhibitor MG-132 or a NEDD8-activating enzyme (NAE) inhibitor MLN4924 (C), followed by a 3 h treatment with **23** at 1 nM in RS4;11 cells.

inducing cell cycle arrest while **23** is very effective at 1−3 nM. We also observed a sharp contrast in their ability to induce apoptosis. While the BET degrader **23** induces robust apoptosis in both RS4;11 and MOLM-13 cell lines at 3−10 nM concentrations with a 24 h treatment, the BET inhibitor **8** is ineffective in both cell lines at concentrations as high as 300 nM.

We tested the antitumor activity of **23** in the RS4;11 xenograft model in mice, and the results are shown in Figure 8. Dosing of the mice bearing RS4;11 xenograft tumors with 5 mg/kg of **23** intravenously every other day, three times a week for 3 weeks, achieved rapid tumor regression with a maximum of >90% regression observed. There was no animal weight loss or other signs of toxicity in mice treated with compound **23**, and the animal weight gained in the vehicle control group of mice was attributed largely to rapid tumor growth. Therefore, the in vivo data firmly establish that **23** has highly efficacious antitumor activity at a well-tolerated dose-schedule in mice.

To gain a better understanding of the strong antitumor activity of **23** and its mechanism of action in vivo, we performed a pharmacodynamics (PD) analysis in SCID mice bearing the RS4;11 xenograft tumors (Figure 9). In this experiment, mice bearing one or two RS4;11 xenograft tumors were administered a single dose of **23** at 5 mg/kg intravenously and were sacrificed at 1, 3, 6, and 24 h time-points after the treatment. Mice treated with vehicle control were sacrificed at the 6 h time point. Western blotting analysis was performed to probe the level of BRD2, BRD3, and BRD4 proteins, as well as c-Myc, caspase-3, and PARP proteins in the tumor tissue. Our PD data (Figure 9) clearly show that a single dose of **23** was highly effective, dramatically reducing the level of BRD2, BRD3, and BRD4 proteins in the RS4;11 tumor tissue, starting from 1 h with the effect persisting for >24 h. The level of c-Myc was strongly down-regulated, with the effect persisting for at least 6 h. Robust cleavage of PARP and caspase-3 was observed, starting from the 3 h time-point and with a peak effect at the 6 h time point, indicating strong apoptosis induction by **23**. Therefore, our PD analysis clearly demonstrates that a single dose of **23** is sufficient to induce near complete degradation of BRD2, BRD3, and BRD4 proteins for >24 h, accompanied by robust cleavage of PARP and caspase-3, and strong down-regulation of c-Myc protein.

We analyzed concentrations of **23** in plasma and also in RS4;11 tumors in the same mice used in the PD experiment (Table 5). Our data showed that despite its relatively large size (MW = 798.8), **23** can effectively penetrate the RS4;11 xenograft tumor tissue and has a concentration of 166.3, 98.5, and 35.8 ng/g in the tumor at 1, 3, and 6 h time-points, respectively, exceeding the drug concentrations needed for effective BET degradation shown in our in vitro experiments (Figures 4 and 5). The drug concentration, however, was undetectable after 24 h. Together with the PD data, our PK data indicate that a single dose of **23** at 5 mg/kg achieves a sufficient exposure in the tumor tissue for effective induction of BET protein degradation for over 24 h.

We also evaluated the metabolism of compound **23** in mouse liver microsomes. The major metabolite was proposed to be mono- or dihydroxylated product occurring in the alkyl chain in the linker. In addition, cleavage of the $C(sp^3)-C(sp^2)$ bond between the linker and cereblon binding ligand and N-deethylation of the pyrazole moiety are other alternative metabolic pathways (for detailed information, see Figure S5).

CHEMISTRY

The synthesis of compounds **8** and **28** is outlined in Scheme 1. Briefly, 3-cyclopropyl-3-oxopropanenitrile (**29**) and ethylhydrazine oxalate (**30**) were heated in EtOH to generate **31**. Compound **32** was prepared as described, and intermediate **33** was obtained from **32** in four steps.[31] Coupling of **31** with **33** followed by hydrolysis of the methyl ester produced the key intermediate **34**. Amidation of **34** with $MeNH_2$ in the presence of 1-[bis(dimethylamino)methylene]-1*H*-1,2,3-triazolo[4,5-*b*]-pyridinium 3-oxide hexafluorophosphate (HATU) and *N*,*N*-diisopropylethylamine (DIPEA) at room temperature in dimethylformamide (DMF) gave the target compound **8**. Compound **36** was formed by dehalogenation of **33** in the presence of Pd/C and H_2, followed by hydrolysis. Acyl chloride formation followed by amidation of **36** generated **28**.

The synthesis of compound **9** is shown in Scheme 2. Condensation of 3-hydroxyphthalic anhydride (**37**) with 3-aminopiperidine-2,6-dione hydrochloride (**38**) afforded the intermediate **39**. Alkylation of **39** with *tert*-butyl bromoacetate generated **40**, which was subjected to trifluoroacetic acid-promoted ester hydrolysis. Amide condensation and Boc-deprotection reactions afforded **41**. Condensation of **41** with **34** under the same conditions described for the synthesis of **8** gave compound **9**.

The synthetic route to compound **10** is shown in Scheme 3. Compound **43** was obtained by treatment of 3-nitrophthalic

DOI: 10.1021/acs.jmedchem.6b01816
J. Med. Chem. 2018, 61, 462−481

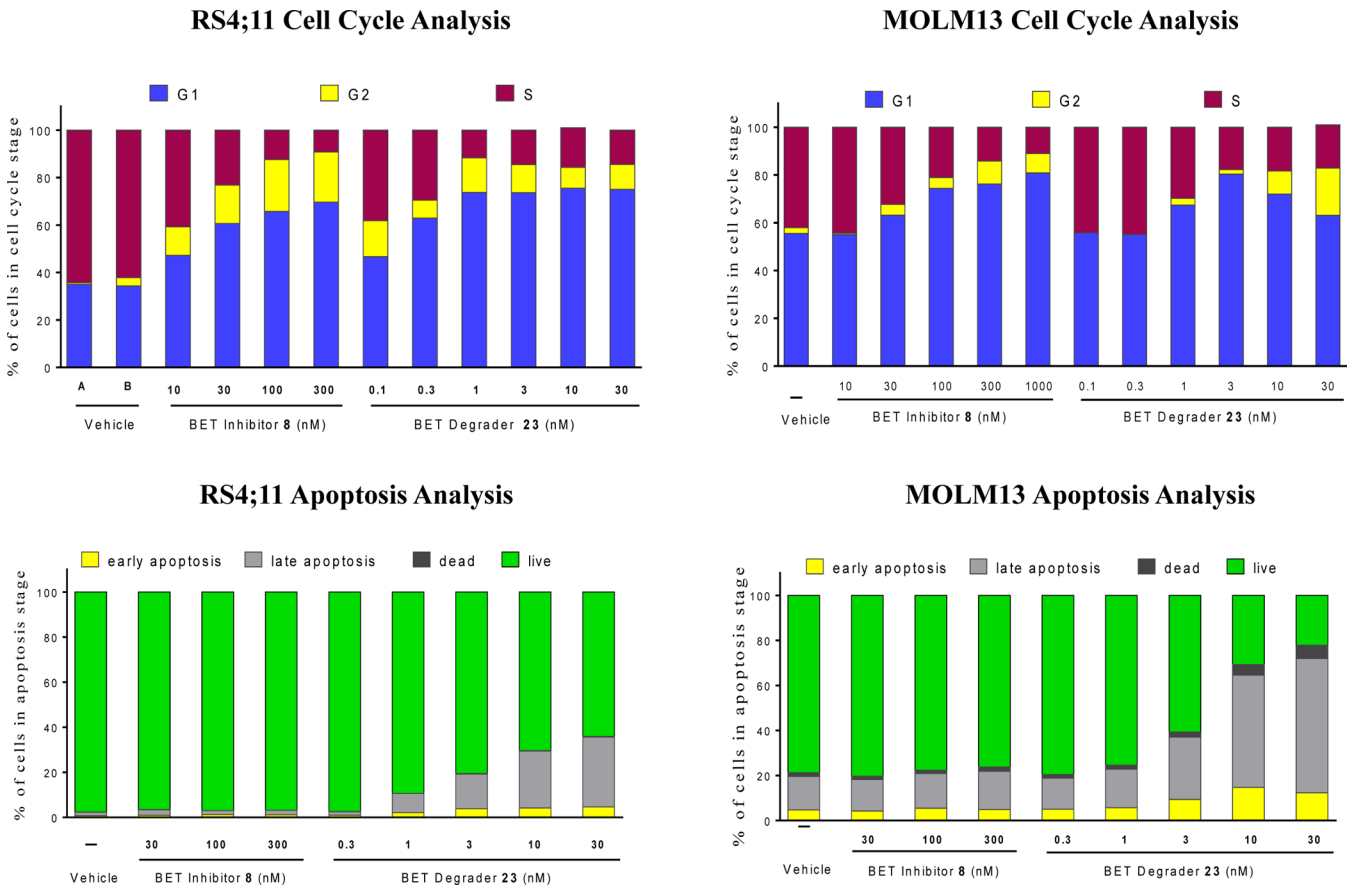

Figure 7. Induction of cell cycle arrest and apoptosis by BET degrader **23** and BET inhibitor **8** in the RS4;11 and MOLM-13 cell lines by flow cytometry analysis.

anhydride (**42**) with benzyl bromide, followed by reduction of the nitro group with stannous chloride dihydrate and alkylation with *tert*-butyl bromoacetate. Removal of the benzyl groups of **43** followed by amide condensation resulted in **44**. Compound **10** was prepared from **44** by the same procedure as was used for the synthesis of **9**.

As shown in Scheme 4, compound **11** was synthesized starting from the intermediate **39**. Alkylation of the hydroxyl group of **39** with 7-bromo-1-heptanol gave **46**. Compound **47** was obtained by conversion of the hydroxyl group to an amine group in **46** through three steps. Condensation of **47** with **34** using previously described methods afforded compound **11**.

Compounds **12**–**17** were synthesized according to the route shown in Scheme 5. Compound **49** was prepared from **48** by the strategy used in the preparation of **39**. Compounds **50a**–**f** were formed by substitution reaction of **49** with different length of mono-Boc protected alkyl diamines. Boc-deprotection with TFA in DCM afforded the intermediates **51a**–**f**, which were subsequently condensed with **34** to generate compounds **12**–**17**.

The synthesis of compounds **18** and **20** is shown in Scheme 6. Sonogashira coupling of **53**, which was prepared in a manner similar to that used to produce **49**, with different terminal alkyne-containing linker substrates gave **54a**,**b**. Reduction of the alkyne group in **54a**,**b** resulted in **55a**,**b**, whose Boc group was removed in TFA/DCM to form **56a**,**b**. Compounds **18** and **20** were obtained by condensation of **56a**,**b** with **34** using the same method as was used for **9**.

Synthesis of compounds **19** and **22** is shown in Scheme 7. Bromination of **57** with *N*-bromosuccinimide (NBS) and benzoyl peroxide (BPO) gave **58**, which was heated with **38** and triethylamine (TEA) in MeCN to generate **59**. Compounds **19** and **22** were prepared starting from **53** and **59**, respectively, in the same way as **53** was converted to **18** and **20**.

Starting from **59**, compounds **21**, **23**–**25**, and **27** were prepared using the procedure outlined in Scheme 8, which is similar to the procedure used in the preparation of **22** from **59**.

Finally, the synthesis of compound **26** is outlined in Scheme 9. Methylation of **59** with MeI yielded **63**. Compound **26** was prepared from **63** by a process similar to that used for the synthesis of **18** and **20** from **53**.

CONCLUSION

Upon the basis of a novel, azacarbazole-containing potent BET inhibitor and thalidomide/lenalidomide, we have designed a new class of PROTAC small-molecule degraders of BET proteins. Through extensive optimization of the linker length and composition, we have obtained a number of highly potent small-molecule BET protein degraders as exemplified by compound **23**. Compound **23** effectively induces degradation of the BET proteins BRD2, BRD3, and BRD4 at concentrations as low as 0.1–0.3 nM with a 3 h treatment in the RS4;11 acute leukemia cell line and is capable of inducing degradation of BRD4 protein at concentrations as low as 30 pM with a 24 h treatment. Compound **23** achieves an IC_{50} value of 51 pM and 2.3 nM in inhibition of cell growth in the RS4;11 and MOLM-

DOI: 10.1021/acs.jmedchem.6b01816
J. Med. Chem. 2018, 61, 462–481

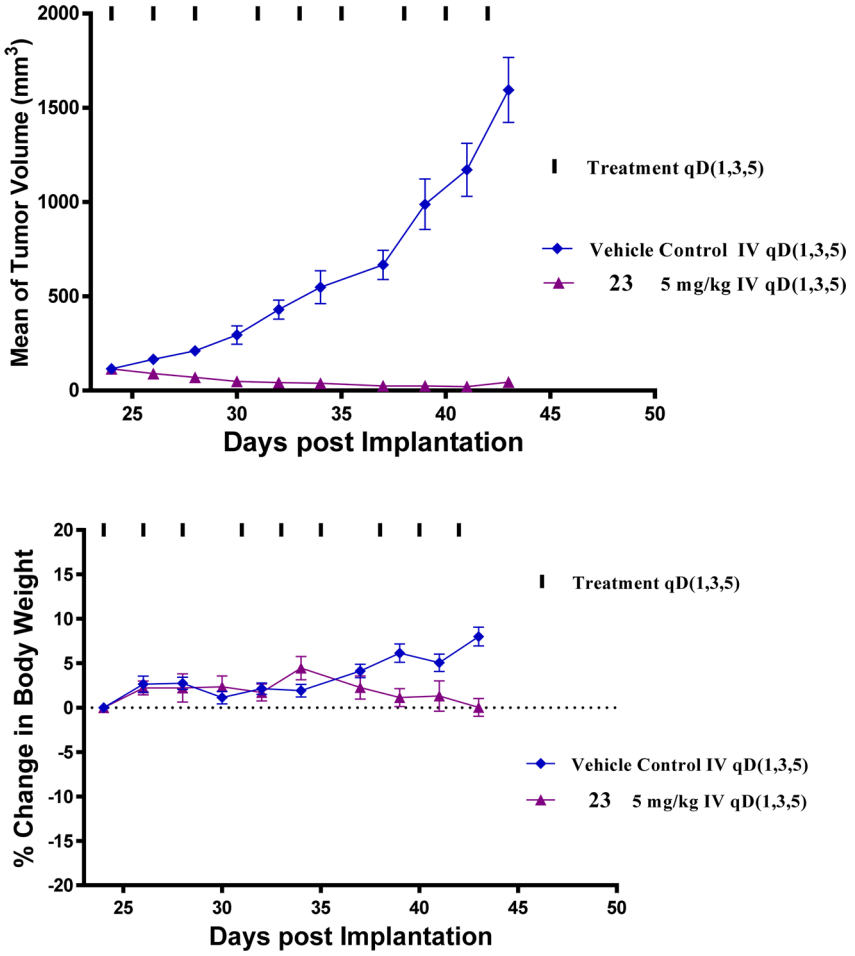

Figure 8. BET degrader **23** induces complete tumor regression in the xenograft model of human RS4;11 tumor cells with minimal body weight change.

13 acute leukemia cell lines, respectively. Our mechanistic investigation firmly establishes that compound **23** is a bona fide PROTAC BET degrader, whose activity requires that **23** binds to BET proteins and the cereblon/Cullin4A E3 ubiquitin ligase complex. Compound **23** effectively induces both cell cycle arrest and apoptosis in RS4;11 and MOLM-13 acute leukemia cell lines at subnanomolar to low nanomolar concentrations. Significantly, **23** achieves >90% tumor regression in the RS4;11 xenograft model in mice at a well-tolerated dose-schedule. Our PD analysis showed that a single, intravenous dose of **23** is capable of inducing profound degradation of BET proteins in the tumor tissue with effect persisting for >24 h, accompanied by robust cleavage of PARP and caspase-3 and strong down-regulation of c-Myc. In addition to its potent anticancer activity against acute leukemia cells, our recent study also showed that compound **23** is very potent and efficacious against triple-negative human breast cancer in vitro and in vivo.[32] Collectively, our data demonstrate that **23** is a highly potent, efficacious, and promising BET degrader and warrants further evaluation as a potential new therapy for the treatment of human acute leukemia and other types of human cancer.

EXPERIMENTAL SECTION

Chemistry. General Experiment and Information. Unless otherwise noted, all purchased reagents were used as received without further purification. ^{1}H NMR and ^{13}C NMR spectra were recorded on a Bruker Advance 400 or 300 MHz spectrometer. ^{1}H NMR spectra were reported in parts per million (ppm) downfield from tetramethylsilane (TMS). All ^{13}C NMR spectra were reported in ppm and obtained with ^{1}H decoupling. In reported spectral data, the format (δ) chemical shift (multiplicity, J values in Hz, integration) was used with the following abbreviations: s = singlet, d = doublet, t = triplet, q = quartet, m = multiplet. MS analyses were carried out with a Waters UPLC−mass spectrometer. The final compounds were all purified by C18 reverse phase preparative HPLC column with solvent A (0.1% TFA in H_2O) and solvent B (0.1% TFA in MeCN) as eluents. The purity of all the final compounds was confirmed to be >95% purity by UPLC−MS or UPLC.

4-((3-Cyclopropyl-1-ethyl-1*H*-pyrazol-5-yl)amino)-7-(3,5-dimethylisoxazol-4-yl)-6-methoxy-*N*-methyl-9*H*-pyrimido[4,5-*b*]indole-2-carboxamide (8). Ethylhydrazine oxalate (**30**, 41.0 g, 0.27 mmol, 1.2 equiv) in 200 mL of EtOH was added to a stirred solution of 3-cyclopropyl-3-oxopropanenitrile (**29**, 25.0 g, 0.23 mol, 1.0 equiv). The resulting solution was heated to reflux for 12 h. After cooling to room temperature, most of the solvent was evaporated. Workup was performed with EtOAc and saturated brine solution. The combined organic layer was dried over anhydrous Na_2SO_4. After filtration and concentration, the residue was purified by flash column chromatography with hexane/EtOAc to afford the desired compound **31** as a slightly yellow solid (22.6 g, 65% yield). ^{1}H NMR (400 MHz, $CDCl_3$) 5.07 (s, 1H), 3.82 (q, J = 7.2 Hz, 2H), 3.55 (s, 2H, NH_2), 1.78−1.71 (m, 1H), 1.28 (t, J = 7.2 Hz, 3H), 0.80−0.75 (m, 2H), 0.57−0.54 (m, 2H). UPLC−MS calculated for $C_8H_{14}N_3$ $[M + H]^+$: 152.12, found 152.09.

Compound 32, Prepared in Three Steps Following a Published Method.[32] Compound **32** (13.16 g, 40 mmol, 1.0 equiv) and ethyl cyanoformate (19.76 mL, 0.2 mol, 5.0 equiv) were

DOI: 10.1021/acs.jmedchem.6b01816
J. Med. Chem. 2018, 61, 462−481

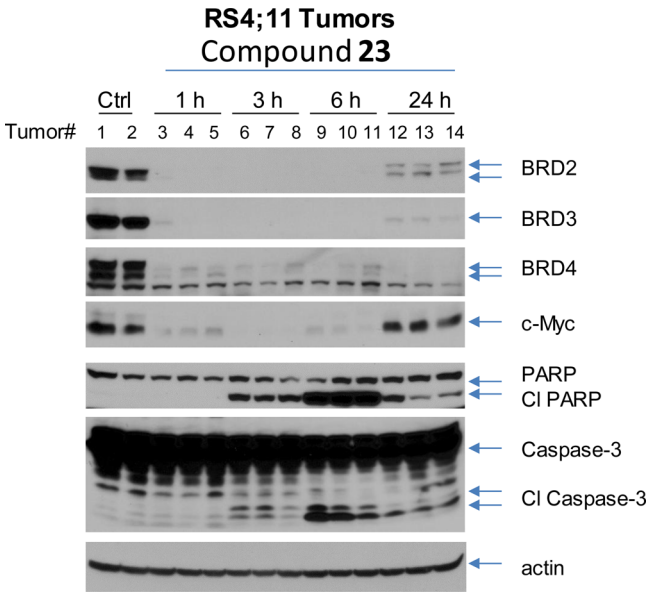

Figure 9. Pharmacodynamic analysis of compound **23** in RS4;11 xenograft tumor tissue. SCID mice bearing RS4;11 tumors were treated with a single intravenous dose of **23** at 5 mg/kg. Mice were sacrificed at 1, 3, 6, and 24 h time-points after administration with compound **23** or at 6 h with vehicle control, and tumors were harvested from mice for Western blotting analysis of BRD2, BRD3, BRD4, c-Myc, PARP and cleaved PARP (Cl PARP), and caspase-3 and cleaved caspase-3 (Cl caspase-3). Actin was used as the loading control. Two mice were used for each time-point with each mouse bearing either one or two tumors.

added to a round-bottom flask at room temperature. A 4.0 M hydrogen chloride solution in dioxane (90 mL) was added, and the reaction mixture was refluxed at 82 °C for 12 h. The reaction was then cooled to room temperature, and the solvents were removed on a rotary evaporator. To this crude mixture, 10% NaOH aqueous solution (120 mL) and EtOH (100 mL) were added, and the solution was heated to reflux for 6 h. The volatile components were then removed on a rotary evaporator, and the aqueous residue was acidified with 2 N aqueous HCl. The product was allowed to precipitate at 0 °C. Filtration of the mixture furnished pure 7-(3,5-dimethylisoxazol-4-yl)-4-hydroxy-6-methoxy-9*H*-pyrimido[4,5-*b*]indole-2-carboxylic acid as a yellow solid (11.34 g, 80% yield). UPLC−MS calculated for $C_{17}H_{15}N_4O_5$ $[M + H]^+$: 355.10, found 355.45.

Concentrated sulfuric acid (15 mL) was added to a solution of 7-(3,5-dimethylisoxazol-4-yl)-4-hydroxy-6-methoxy-9*H*-pyrimido[4,5-*b*]-indole-2-carboxylic acid (11.34 g, 32 mmol) in EtOH (300 mL) in a round-bottom flask. The mixture was heated to reflux for 12 h. The volatile components were removed on a rotary evaporator. Then 400 mL of EtOAc was added. The product was allowed to precipitate. Filtration of the mixture furnished pure methyl 7-(3,5-dimethylisoxazol-4-yl)-4-hydroxy-6-methoxy-9*H*-pyrimido[4,5-*b*]indole-2-carboxylate as a solid (10.61 g, 90% yield). ^{1}H NMR (300 MHz, CD_3OD) δ (ppm) 7.86 (s, 1H), 7.39 (s, 1H), 4.07 (s, 3H), 3.93 (s, 3H), 2.34 (s, 3H), 2.17 (s, 3H).

Methyl 7-(3,5-dimethylisoxazol-4-yl)-4-hydroxy-6-methoxy-9*H*-pyrimido[4,5-*b*]indole-2-carboxylate (10.61 g, 28.8 mmol) and $POCl_3$ (200 mL) were stirred in a round-bottom flask at 90 °C for 12 h, then cooled to room temperature, and the volatile components were removed on a rotary evaporator. EtOAc (200 mL) was added, and the pH was adjusted to 8 using aqueous NaOH solution. Filtration of the mixture furnished compound **33** as a yellow solid (7.80 g, 70% yield). ^{1}H NMR (400 MHz, DMSO-d_6) δ (ppm) 7.81 (s, 1H), 7.55 (s, 1H), 3.92 (s, 3H), 3.90 (s, 3H), 2.33 (s, 3H), 2.12 (s, 3H). UPLC−MS calculated for $C_{18}H_{16}ClN_4O_4$ $[M + H]^+$: 387.09, found 387.18.

$Pd_2(dba)_3$ (183 mg, 0.2 mmol, 0.1 equiv), racemic BINAP (249 mg, 0.4 mmol, 0.2 equiv), and K_3PO_4 (1.70 g, 8.0 mmol, 4.0 equiv) were added sequentially to a solution of compound **33** (774 mg, 2.0 mmol, 1.0 equiv) in toluene (25 mL). The solution was purged and refilled with nitrogen three times before compound **31** (604 mg, 4.0 mmol, 2.0 equiv) was added. The solution was purged and refilled with nitrogen again. The resulting solution was heated to 110 °C and stirred for 12 h. After cooling to room temperature, the solution was filtered through Celite and concentrated. The residue was purified by flash column chromatography with DCM/MeOH to afford methyl 4-((3-cyclopropyl-1-ethyl-1*H*-pyrazol-5-yl)amino)-7-(3,5-dimethylisoxazol-4-yl)-6-methoxy-9*H*-pyrimido[4,5-*b*]indole-2-carboxylate as a yellow solid (702 mg, 70% yield). ^{1}H NMR (400 MHz, DMSO-d_6) 12.15 (s, 1H), 12.05 (s, 1H), 8.06 (s, 1H), 7.56 (s, 1H), 7.22 (s, 1H), 3.99 (q, J = 7.2 Hz, 2H), 3.79 (s, 3H), 3.13 (s, 3H), 2.24 (s, 3H), 2.05 (s, 3H), 1.78−1.71 (m, 1H), 1.14 (t, J = 7.2 Hz, 3H), 0.80−0.75 (m, 2H), 0.57−0.54 (m, 2H).

LiOH (101 mg, 4.2 mmol, 3.0 equiv) was added to a solution of methyl 4-((3-cyclopropyl-1-ethyl-1*H*-pyrazol-5-yl)amino)-7-(3,5-dimethylisoxazol-4-yl)-6-methoxy-9*H*-pyrimido[4,5-*b*]indole-2-carboxylate (702 mg, 1.4 mmol, 1.0 equiv) in THF (20 mL). The solution was stirred at room temperature for 12 h. After concentration, the residue was purified by preparative HPLC to afford the desired compound **34** as a yellow solid (545 mg, 80% yield).

HATU (27 mg, 0.07 mmol, 1.4 equiv), DIPEA (27 μL, 0.15 mmol, 3.0 equiv), and methylamine (2.0 M in THF 0.1 mL, 0.20 mmol, 4.0 equiv) were added sequentially to a stirred solution of compound **34** (24 mg, 0.05 mmol, 1.0 equiv) in DMF (2.0 mL). The solution was stirred at room temperature for 2 h. Preparative HPLC afforded the pure product (**8**) as a slightly yellow solid (17 mg, 68% yield). ^{1}H NMR (400 MHz, DMSO-d_6) δ (ppm) 12.17 (s, 1H), 9.27 (s, 1H), 8.21 (s, 1H), 7.43 (s, 1H), 7.34 (s, 1H), 5.92 (s, 1H), 3.96 (q, J = 7.2 Hz, 2H), 3.81 (s, 3H), 2.81 (d, J = 4.8 Hz, 3H), 2.30 (s, 3H), 2.09 (s, 3H), 1.92−1.85 (m, 1H), 1.32 (t, J = 7.2 Hz, 3H), 0.87−0.82 (m, 2H), 0.64−0.60 (m, 2H). UPLC−MS calculated for $C_{26}H_{29}N_8O_3$ $[M + H]^+$: 501.24, found 501.22. Purity, 99.0%.

4-((3-Cyclopropyl-1-ethyl-1*H*-pyrazol-5-yl)amino)-7-(3,5-dimethylisoxazol-4-yl)-*N*-(4-(2-((2-(2,6-dioxopiperidin-3-yl)-1,3-dioxoisoindolin-4-yl)oxy)acetamido)butyl)-6-methoxy-9*H*-pyrimido[4,5-*b*]indole-2-carboxamide (9). In a round-bottom flask, 3-hydroxyphthalic anhydride **37** (1.0 g, 6.09 mmol, 1.0 equiv) and 3-aminoperidine-2,6-dione hydrochloride **38** (1.0 g, 6.09 mmol, 1.0 equiv) were mixed in toluene (50 mL). TEA (0.93 mL, 6.7 mmol,

Table 5. Analysis of Concentrations of Compound 23 in Plasma and RS4;11 Tumor Tissue[a]

	concn in plasma (ng/mL)			concn in tumor (ng/g)				
time-point (h)	individual mice		mean	individual tumor			mean	SD
1	422	362	392	135.5	123	240.5	166.3	64.5
3	58	76.1	67.1	86	89	120.5	98.5	19.1
6	5.5	7.4	6.4	39.4	31.9	36.2	35.8	3.8
24	<1	<1	<1	<1	<1	<1	<1	

[a]Mice bearing RS4;11 xenograft tumors were administered with a single dose of compound **23** at 5 mg/kg intravenously. Mice were sacrificed at 1, 3, 6, and 24 h time-points after administration with compound **23**, and plasma and tumor tissue were collected for analysis. Two mice were used for each time-point with each mouse bearing either one or two tumors (three tumors for each time point).

DOI: 10.1021/acs.jmedchem.6b01816
J. Med. Chem. 2018, 61, 462−481

Scheme 1. Compounds 8 and 28[a]

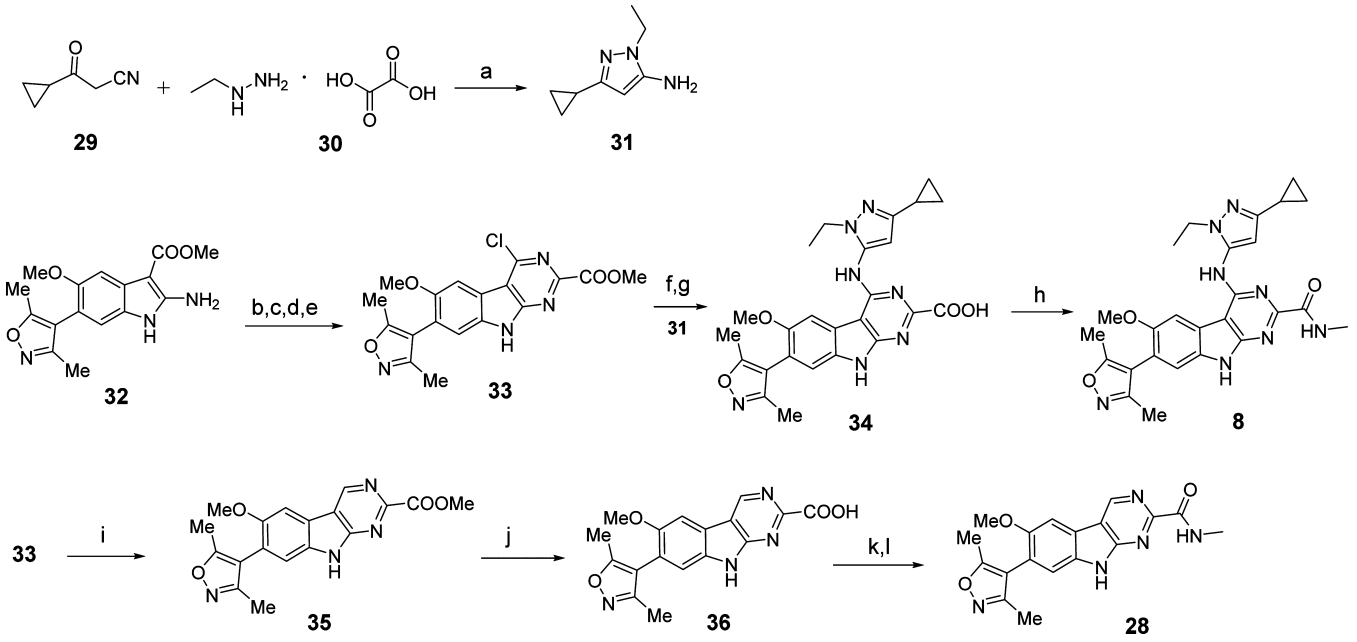

[a]Reaction conditions: (a) EtOH, reflux; (b) NCCOOEt, 4 N HCl in dioxane; (c) 10% NaOH (aq), EtOH, reflux; (d) conc H_2SO_4, MeOH, reflux; (e) $POCl_3$, reflux; (f) $Pd_2(dba)_3$, BINAP, K_3PO_4, toluene, reflux; (g) LiOH, THF, rt; (h) NH_2Me, HATU, DIPEA, DMF, rt; (i) Pd/C, H_2, DMF, 60 °C; (j) LiOH, THF, rt; (k) 2 drops of DMF, $SOCl_2$, reflux; (l) methylamine hydrochloride, THF, rt.

Scheme 2. Compound 9[a]

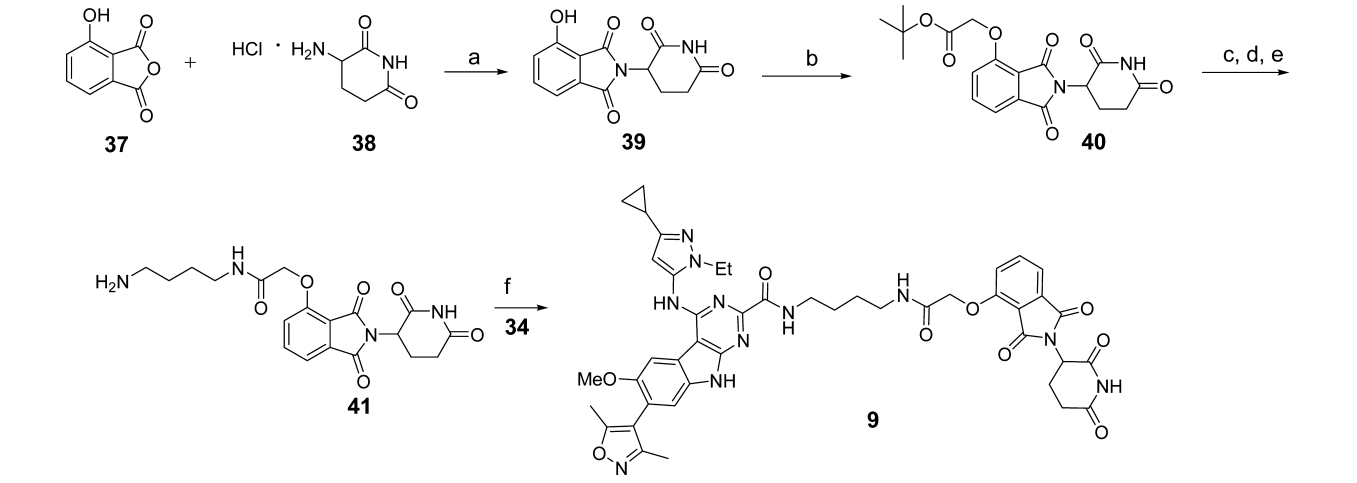

[a]Reaction conditions: (a) TEA, toluene, reflux; (b) *tert*-butyl bromoacetate, KI, $KHCO_3$, DMF, 60 °C; (c) TFA, rt; (d) *N*-Boc-1,4-butanediamine, HATU, DIPEA, DMF, rt; (e) TFA, DCM, rt; (f) HATU, DIPEA, DMF, rt.

1.1 equiv) was added. The resulting reaction mixture was heated to reflux for 12 h with Dean−Stark trap equipment. After cooling to ambient temperature, evaporation of most of the solvent afforded a crude product, which was purified by flash column chromatography with DCM/MeOH to obtain the desired product **39** as a slightly yellow solid (1.5 g, 90% yield). ^{1}H NMR (400 MHz, DMSO-d_6) δ (ppm) 11.16 (s, 1H), 11.08 (s, 1H), 7.65 (t, J = 7.6 Hz, 1H), 7.32 (d, J = 7.2 Hz, 1H), 7.25 (d, J = 8.4 Hz, 1H), 5.07 (dd, J = 12.8 Hz, J = 5.2 Hz, 1H), 2.93−2.84 (m, 1H), 2.61−2.46 (m, 1H), 2.05−2.01 (m, 1H); ^{13}C NMR (100 MHz, DMSO-d_6) δ (ppm) 173.28, 170.48, 167.50, 166.30, 155.99, 136.83, 133.60, 124.05, 114.82, 114.72, 49.11, 31.43, 22.51.

In a round-bottom flask, compound **39** (1.5 g, 5.5 mmol, 1.0 equiv) was dissolved in DMF (10 mL). KI (91 mg, 0.55 mmol, 0.1 equiv) and $KHCO_3$ (826 mg, 8.25 mmol, 1.5 equiv) were added to the stirred solution. Then *tert*-butyl bromoacetate (0.98 mL, 6.6 mmol, 1.2 equiv) was added dropwise. The resulting mixture was stirred at 60 °C for 12 h. After normal workup with EtOAc and saturated brine, the combined organic layer was dried over Na_2SO_4. After filtration and evaporation, the residue was purified by flash column chromatography with DCM/MeOH to get the intermediate **40** as a white solid (1.7 g, 80% yield). ^{1}H NMR (400 MHz, DMSO-d_6) δ (ppm) 11.13 (s, 1H), 7.80 (t, J = 8.0 Hz, 1H), 7.48 (d, J = 7.2 Hz, 1H), 7.38 (d, J = 8.4 Hz, 1H), 5.13 (dd, J = 12.8 Hz, J = 5.2 Hz, 1H), 4.97 (s, 2H), 2.97−2.85 (m, 1H), 2.65−2.52 (m, 2H), 2.14−2.03 (m, 1H), 1.43 (s, 9H).

The intermediate **40** was dissolved in TFA (8.0 mL). The reaction mixture was stirred at room temperature for 2 h. After evaporation of the solvent, the residue was freeze-dried on a lyophilizer to afford a white solid, which was used in the following steps without further purification. ^{1}H NMR (400 MHz, DMSO-d_6) δ (ppm) 13.16 (s, 1H), 11.11 (s, 1H), 7.80 (t, J = 8.0 Hz, 1H), 7.48 (d, J = 7.2 Hz, 1H), 7.40 (d, J = 8.8 Hz, 1H), 5.11 (dd, J = 12.8 Hz, J = 5.2 Hz, 1H), 4.99 (s,

DOI: 10.1021/acs.jmedchem.6b01816
J. Med. Chem. 2018, 61, 462−481

Scheme 3. Compound 10[a]

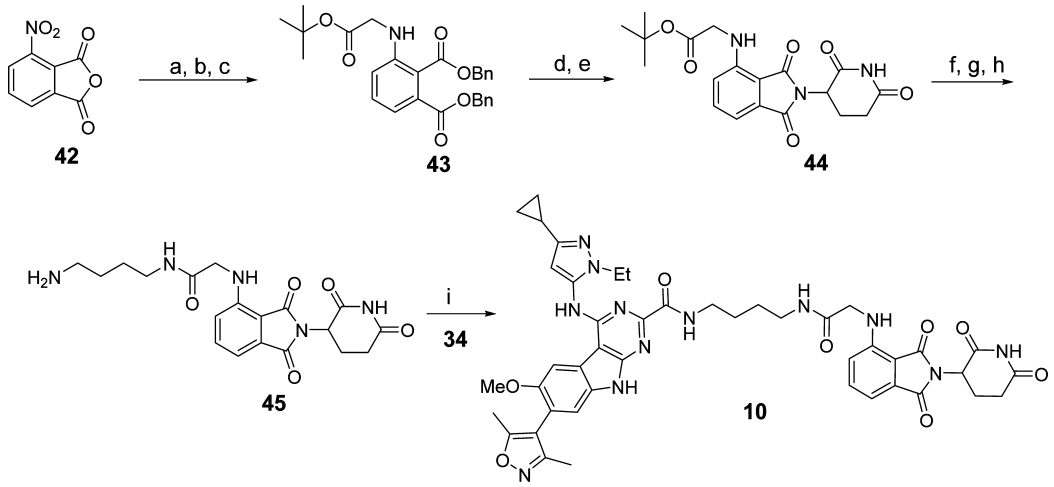

[a]Reaction conditions: (a) $TsOH·H_2O$, BnOH, 100 °C; BnBr, $NaHCO_3$, DMF, 100 °C; (b) $SnCl_2·2H_2O$, EtOAc, 50 °C; (c) *tert*-butyl bromoacetate, DIPEA, DMF, 90 °C; (d) Pd/C, H_2, EtOH, rt; (e) **38**, pyridine, 110 °C; (f) TFA, rt; (g) *N*-Boc-1,4-butanediamine, HATU, DIPEA, DMF, rt; (h) TFA, DCM, rt; (i) HATU, DIPEA, DMF, rt.

Scheme 4. Compound 11[a]

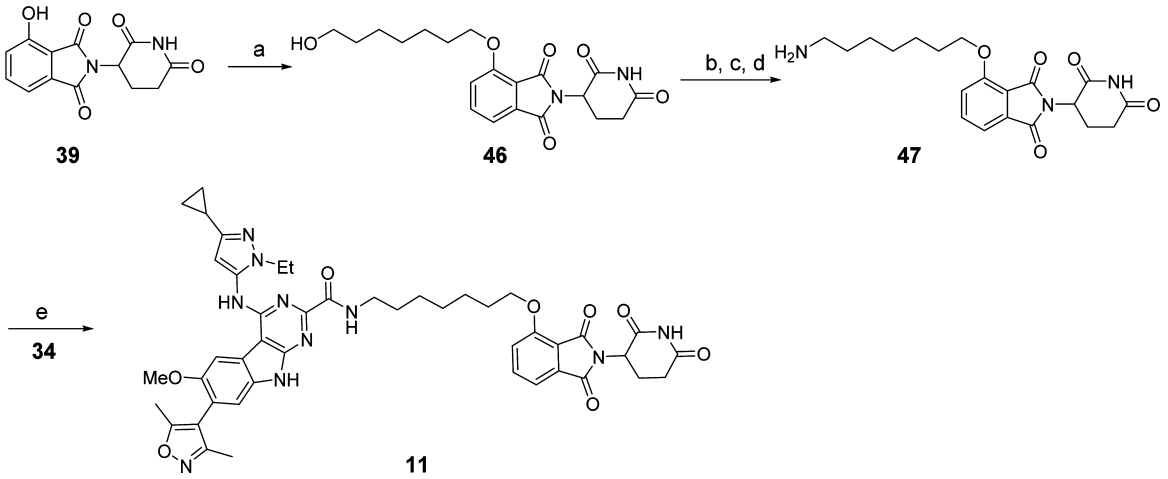

[a]Reaction conditions: (a) 7-bromoheptan-1-ol, $NaHCO_3$, KI, DMF, 80 °C; (b) MsCl, TEA, DCM; (c) NaN_3, DMF, 80 °C; (d) PPh_3, THF/H_2O, rt; (e) HATU, DIPEA, DMF, rt.

2H), 2.95−2.86 (m, 1H), 2.63−2.48 (m, 2H), 2.08−2.03 (m, 1H); ^{13}C NMR (100 MHz, DMSO-d_6) δ (ppm) 173.26, 170.38, 169.97, 167.21, 165.64, 155.61, 137.23, 133.73, 120.35, 116.80, 116.23, 65.48, 49.27, 31.42, 22.44. UPLC−MS calculated for $C_{15}H_{13}N_2O_7$ $[M + H]^+$: 333.07, found 333.17.

In a round-bottom flask, the intermediate obtained from the previous step (99.7 mg, 0.3 mmol, 1.0 equiv) was dissolved in anhydrous DMF (2 mL). *N*-Boc-1,4-butanediamine (68 mg, 0.36 mmol, 1.2 equiv), HATU (137 mg, 0.36 mmol, 1.2 equiv), and DIPEA (157 μL, 0.9 mmol, 3.0 equiv) were added sequentially. The reaction mixture was stirred at room temperature for 2 h and then purified by HPLC to get the product as a slightly yellow solid (128 mg, 85% yield) which was dissolved in DCM (2.0 mL) and TFA (1.0 mL). After stirring for 1 h, the solvent was evaporated and the residue **41** was used as a stored solution (0.1 M in DMF) in the next step without further purification.

HATU (27 mg, 0.07 mmol, 1.4 equiv), DIPEA (27 μL, 0.15 mmol, 3.0 equiv), and the amine intermediate **41** (0.1 M in DMF 0.7 mL, 0.07 mmol, 1.4 equiv) were added sequentially to a stirred solution of compound **34** (24 mg, 0.05 mmol, 1.0 equiv) in DMF (2.0 mL). The solution was then stirred at room temperature for 2 h. Preparative HPLC purification afforded the pure product (**9**) as a slightly yellow solid (27 mg, 63% yield). ^1H NMR (400 MHz, DMSO-d_6) δ (ppm) 12.21 (s, 1H), 11.10 (s, 1H), 9.30 (s, 1H), 8.23 (t, J = 6.0 Hz, 1H), 8.00 (t, J = 6.0 Hz, 1H), 7.81 (t, J = 7.6 Hz, 1H), 7.47 (d, J = 7.2 Hz, 1H), 7.39 (d, J = 8.4 Hz, 1H), 7.34 (s, 1H), 5.93 (s, 1H), 5.11 (dd, J = 12.8 Hz, J = 5.2 Hz, 1H), 4.78 (s, 2H), 3.95 (q, J = 7.2 Hz, 2H), 3.82 (s, 3H), 3.30−3.25 (m, 2H), 3.22−3.16 (m, 2H), 2.89−2.85 (m, 1H), 2.60−2.45 (m, 2H), 2.30 (s, 3H), 2.10 (s, 3H), 2.05−2.01 (m, 1H), 1.90−1.85 (m, 1H), 1.51−1.49 (m, 4H), 1.31 (t, J = 7.2 Hz, 3H), 0.86−0.81 (m, 2H), 0.63−0.60 (m, 2H). UPLC−MS calculated for $C_{44}H_{46}N_{11}O_9$ $[M + H]^+$: 872.35, found 872.37. Purity, >99.0%.

4-((3-Cyclopropyl-1-ethyl-1*H*-pyrazol-5-yl)amino)-7-(3,5-dimethylisoxazol-4-yl)-*N*-(4-(2-((2-(2,6-dioxopiperidin-3-yl)-1,3-dioxoisoindolin-4-yl)amino)acetamido)butyl)-6-methoxy-9*H*-pyrimido[4,5-*b*]indole-2-carboxamide (10). In a round-bottom flask, 3-nitrophthalic anhydride **42** (5.79 g, 30 mmol, 1.0 equiv) and *p*-toluenesulfonic acid monohydrate (571 mg, 3 mmol, 0.1 equiv) were mixed in benzyl alcohol (20 mL). The mixture was heated to 100 °C and stirred for 12 h. After cooling to room temperature, benzyl bromide (7.1 mL, 45 mmol, 1.5 equiv), KI (498 mg, 3 mmol, 0.1 equiv), $KHCO_3$ (9.0 g, 90 mmol, 3.0 equiv), and DMF (25 mL) were added. The mixture was heated to 100 °C and stirred for 6 h. After cooling to room temperature, the solvent was evaporated and the

DOI: 10.1021/acs.jmedchem.6b01816
J. Med. Chem. 2018, 61, 462−481

Scheme 5. Compounds 12−17[a]

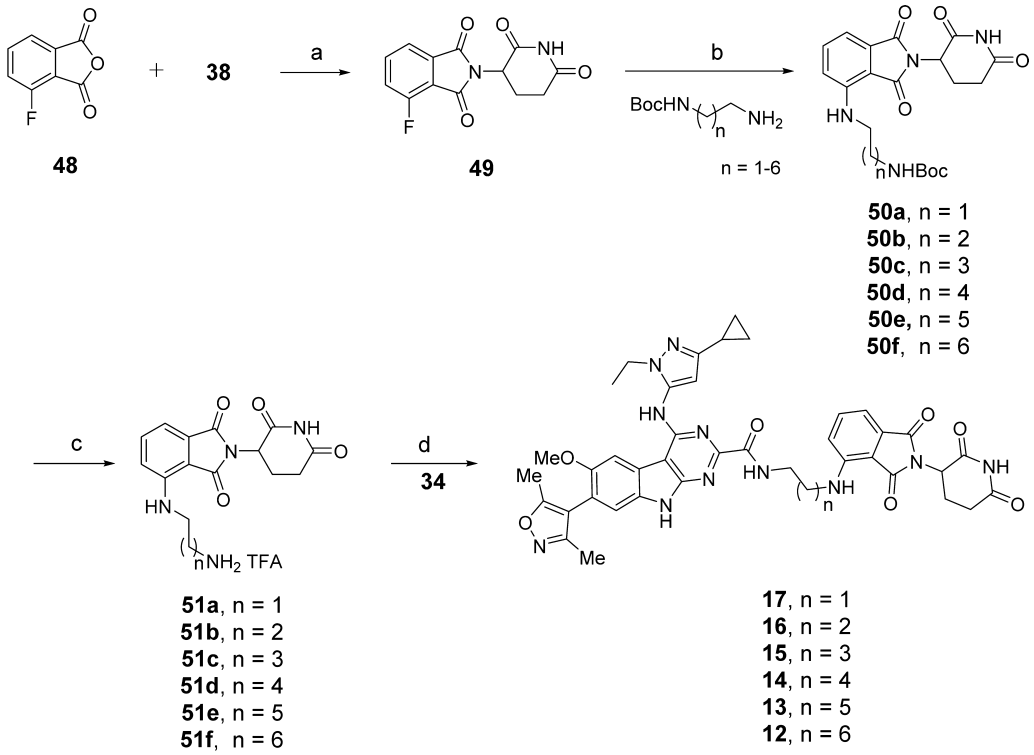

[a]Reaction conditions: (a) NaOAc, AcOH, reflux; (b) DIPEA, DMF, 80 °C; (c) TFA, DCM, rt; (d) HATU, DIPEA, DMF, rt.

Scheme 6. Compounds 18 and 20[a]

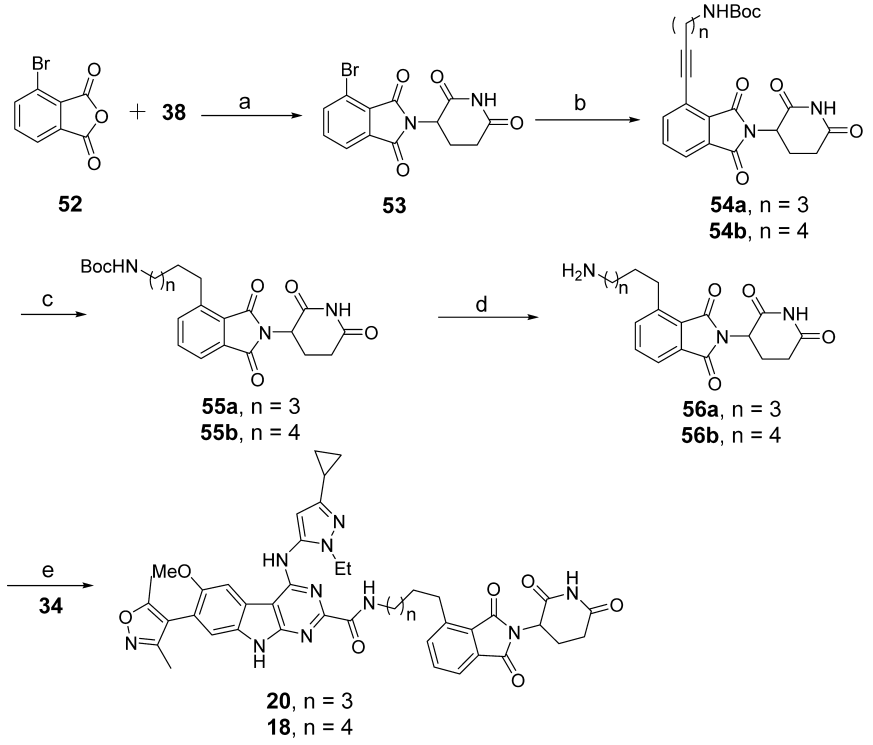

[a]Reaction conditions: (a) NaOAc, AcOH; (b) *tert*-butyl pent-4-yn-1-ylcarbamate or *tert*-butyl hex-5-yn-1-ylcarbamate, $Pd(PPh_3)_2Cl_2$, CuI, DMF/TEA, 80 °C; (c) Pd/C, H_2, EtOH, rt; (d) TFA, DCM, rt; (e) HATU, DIPEA, DMF, rt.

mixture was then poured into H_2O (300 mL). The solution was extracted with EtOAc. The combined organic layers were washed with brine and dried over anhydrous Na_2SO_4. After filtration and evaporation, the crude residue was purified by flash column chromatography with hexane/EtOAc to give the intermediate dibenzyl 3-nitrophthalate as a slightly yellow solid (9.4 g, 80% yield).

DOI: 10.1021/acs.jmedchem.6b01816
J. Med. Chem. 2018, 61, 462−481

Scheme 7. Compounds 19 and 22[a]

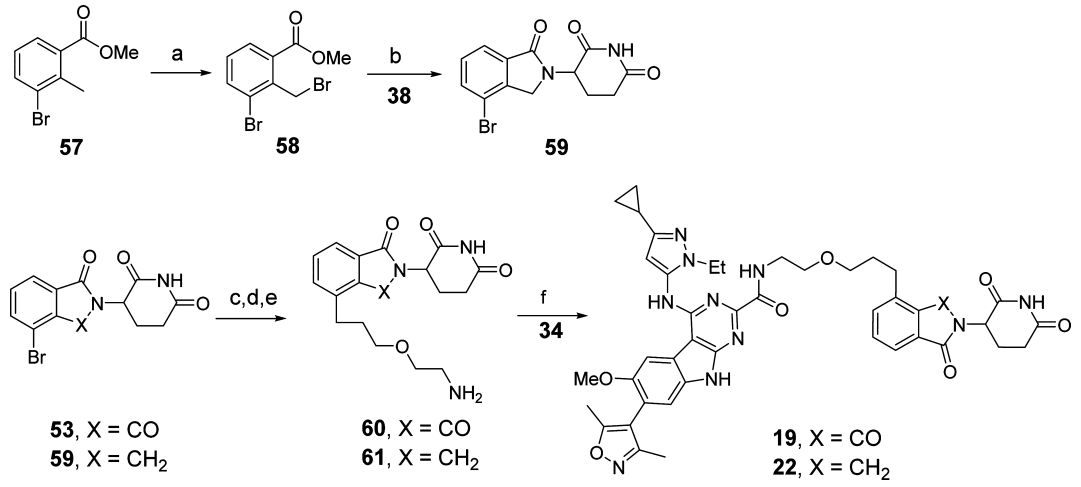

[a]Reaction conditions: (a) NBS, BPO, benzene, reflux; (b) TEA, MeCN, reflux; (c) *tert*-butyl (2-(prop-2-yn-1-yloxy)ethyl)carbamate, $Pd(PPh_3)_2Cl_2$, CuI, DMF/TEA, 80 °C; (d) Pd/C, H_2, EtOH, rt; (e) TFA, DCM, rt; (f) HATU, DIPEA, DMF, rt.

Scheme 8. Compounds 21, 23−25, and 27[a]

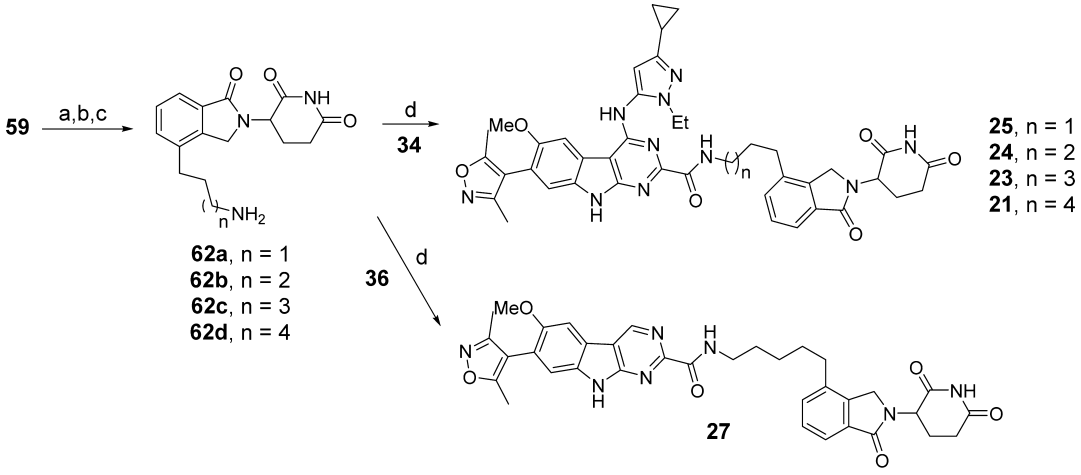

[a]Reaction conditions: (a) *tert*-butyl prop-2-yn-1-ylcarbamate or *tert*-butyl but-3-yn-1-ylcarbamate or *tert*-butyl pent-4-yn-1-ylcarbamate or *tert*-butyl hex-5-yn-1-ylcarbamate, $Pd(PPh_3)_2Cl_2$, CuI, DMF/TEA, 80 °C; (b) Pd/C, H_2, EtOH, rt; (c) TFA, DCM, rt; (d) HATU, DIPEA, DMF, rt.

Scheme 9. Compound 26[a]

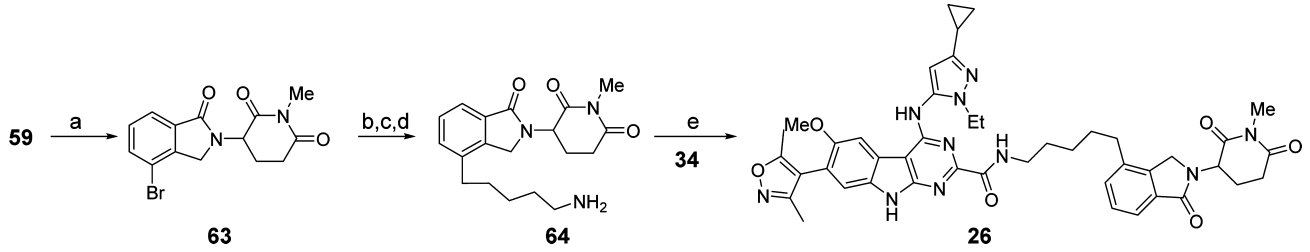

[a]Reaction conditions: (a) MeI, K_2CO_3, DMF, 60 °C; (b) *tert*-butyl pent-4-yn-1-ylcarbamate, $Pd(PPh_3)_2Cl_2$, CuI, DMF/TEA, 80 °C; (c) Pd/C, H_2, EtOH, rt; (d) TFA, DCM, rt; (e) HATU, DIPEA, DMF, rt.

In a round-bottom flask, dibenzyl 3-nitrophthalate (9.4 g, 24 mmol, 1.0 equiv) was dissolved in EtOAc (100 mL). Then stannous chloride dihydrate (11.3 g, 50 mmol, 2.08 equiv) was added portionwise to the reaction mixture. The resulting reaction mixture was heated to 50 °C and stirred for 12 h. Then NaOH (aq) was added to the reaction mixture to quench the reaction. The reaction mixture was filtered through Celite and washed with EtOAc. The filtrate was extracted with EtOAc and brine. The combined organic layer was dried over anhydrous Na_2SO_4. After filtration and evaporation, the crude residue was purified by flash column chromatography with hexane/EtOAc to give dibenzyl 3-aminophthalate as a slightly yellow solid (7.8 g, 90% yield). ^1H NMR (400 MHz, $CDCl_3$) δ (ppm) 7.45−7.36 (m, 10H), 7.22 (t, J = 8.4 Hz, 1H), 6.96 (d, J = 7.2 Hz, 1H), 6.76 (d, J = 7.6 Hz, 1H), 5.36 (s, 2H, NH_2), 5.26 (s, 2H), 5.10 (s, 2H).

In a round-bottom flask, dibenzyl 3-aminophthalate (2.0 g, 5.54 mmol, 1.0 equiv) and KI (100 mg, 0.56 mmol, 0.1 equiv) were

DOI: 10.1021/acs.jmedchem.6b01816
J. Med. Chem. 2018, 61, 462−481

combined with anhydrous DMF (10 mL). *tert*-Butyl bromoacetate (2.4 mL, 16.6 mmol, 3.0 equiv) and DIPEA (4.8 mL, 27.7 mmol, 5.0 equiv) were added to the reaction mixture which was then heated to 90 °C and stirred for 12 h. After cooling to room temperature, most of the solvent was evaporated and the residue was purified by column chromatography with hexane/EtOAc to give compound **43** as a slightly yellow solid (1.05 g, 40% yield). ^{1}H NMR (400 MHz, $CDCl_3$) δ (ppm) 7.40−7.25 (m, 11H), 6.87 (d, J = 7.2 Hz, 1H), 6.65 (d, J = 8.4 Hz, 1H), 5.20 (s, 2H), 4.95 (s, 2H), 3.88 (d, J = 4.8 Hz, 2H), 1.52 (s, 9H); ^{13}C NMR (100 MHz, $CDCl_3$) δ (ppm) 169.16, 168.86, 167.61, 148.44, 135.78, 135.66, 135.42, 132.82, 128.72, 128.62, 128.58, 128.40, 128.22, 128.16, 116.54, 113.89, 111.32, 82.38, 67.32, 66.97, 46.07, 28.27.

In a round-bottom flask, compound **43** (1.0 g, 2.1 mmol) was dissolved in EtOH (20 mL). 100 mg of Pd/C (10 wt %) was added under N_2. The flask was purged and refilled with H_2 three times. Then the reaction mixture was stirred at room temperature under 1 atm of H_2. Once the starting material disappeared, as judged by TLC, the mixture was filtered through Celite and washed with EtOH. After evaporation of the solvent, 3-aminopiperidine-2,6-dione hydrochloride **38** (380 mg, 2.31 mmol, 1.1 equiv) and pyridine (20 mL) were added. The reaction mixture was heated to 110 °C and stirred overnight. After cooling to room temperature, the solvent was evaporated as much as possible and the residue was poured into H_2O. After extraction three times with EtOAc, the combined organic layer was washed with brine and dried over anhydrous Na_2SO_4. After filtration and evaporation, the crude residue was purified by flash column chromatography with DCM/MeOH to give compound **44** as a yellow solid (325 mg, 40% yield).

TFA (2.0 mL) was added to compound **44**, obtained as described above. The intermediate (2-(2,6-dioxopiperidin-3-yl)-1,3-dioxoisoindolin-4-yl)glycine was obtained by evaporation of the solvent without further purification. ^{1}H NMR (400 MHz, DMSO-d_6) δ (ppm) 12.91 (s, 1H, COOH), 11.10 (s, 1H, NH), 7.59 (t, J = 7.6 Hz, 1H), 7.08 (d, J = 6.8 Hz, 1H), 6.99 (d, J = 8.4 Hz, 1H), 6.86 (t, J = 5.6 Hz, 1H, NH), 5.08 (dd, J = 13.2 Hz, J = 5.6 Hz, 1H), 4.12 (d, J = 5.2 Hz, 2H), 2.94−2.85 (m, 1H), 2.63−2.49 (m, 2H), 2.09−2.07 (m, 1H); ^{13}C NMR (100 MHz, DMSO-d_6) δ (ppm) 173.28, 171.90, 170.52, 169.26, 167.75, 146.28, 136.60, 132.48, 118.18, 111.54, 110.11, 60.22, 49.07, 31.46, 22.61. UPLC−MS calculated for $C_{15}H_{14}N_3O_6$ $[M + 1]^+$: 332.09, found 332.00.

Following the procedure for the synthesis of compound **41**, compound **45** (250 mg, 0.76 mmol) was synthesized from the intermediate (2-(2,6-dioxopiperidin-3-yl)-1,3-dioxoisoindolin-4-yl)-glycine.

HATU (27 mg, 0.07 mmol, 1.4 equiv), DIPEA (27 μL, 0.15 mmol, 3.0 equiv), and compound **45** (28 mg, 0.07 mmol, 1.4 equiv) were added sequentially to a stirred solution of compound **34** (24 mg, 0.05 mmol, 1.0 equiv) in DMF (2.0 mL). The solution was stirred at room temperature for 2 h. Preparative HPLC purification afforded the pure product (**10**) as a slightly yellow solid (32 mg, 75% yield). ^{1}H NMR (400 MHz, DMSO-d_6) δ (ppm) 12.32 (s, 1H), 11.09 (s, 1H), 9.41 (s, 1H), 8.26 (t, J = 5.6 Hz, 1H), 8.19 (t, J = 5.6 Hz, 1H), 7.58 (t, J = 8.0 Hz, 1H), 7.48 (s, 1H), 7.41 (s, 1H), 7.03 (d, J = 6.8 Hz, 1H), 6.87 (d, J = 8.8 Hz, 1H), 5.94 (s, 1H), 5.07 (dd, J = 12.8 Hz, J = 5.6 Hz, 1H), 3.97 (q, J = 7.2 Hz, 2H), 3.94 (s, 2H), 3.82 (s, 3H), 3.29−3.26 (m, 2H), 3.15−3.12 (m, 2H), 2.93−2.84 (m, 1H), 2.61−2.45 (m, 2H), 2.30 (s, 3H), 2.10 (s, 3H), 2.05−2.01 (m, 1H), 1.92−1.85 (m, 1H), 1.51−1.45 (m, 4H), 1.31 (t, J = 7.2 Hz, 3H), 0.87−0.82 (m, 2H), 0.64−0.60 (m, 2H). UPLC−MS calculated for $C_{44}H_{47}N_{12}O_8$ $[M + H]^+$: 871.36, found 871.39. Purity, 91.4%.

4-((3-Cyclopropyl-1-ethyl-1*H*-pyrazol-5-yl)amino)-7-(3,5-dimethylisoxazol-4-yl)-*N*-(7-((2-(2,6-dioxopiperidin-3-yl)-1,3-dioxoisoindolin-4-yl)oxy)heptyl)-6-methoxy-9*H*-pyrimido[4,5-*b*]indole-2-carboxamide (11). KI (33 mg, 0.2 mmol, 0.1 equiv), $NaHCO_3$ (336 mg, 4.0 mmol, 2.0 equiv), and 7-bromo-1-heptanol (468 mg, 2.4 mmol, 1.2 equiv) were added sequentially to a solution of compound **39** (548 mg, 2.0 mmol, 1.0 equiv) in DMF (10 mL). The resulting solution was heated to 60 °C and stirred for 12 h. After cooling to room temperature, the solution was filtered through Celite and concentrated. The residue was purified by preparative HPLC to afford **46** as a colorless solid (589 mg, 76% yield). ^{1}H NMR (400 MHz, DMSO-d_6) δ (ppm) 11.10 (s, 1H), 7.80 (t, J = 7.80 Hz, 1H), 7.51 (d, J = 8.4 Hz, 1H), 7.44 (d, J = 7.2 Hz, 1H), 5.09 (dd, J = 12.8 Hz, J = 5.2 Hz, 1H), 4.20 (t, J = 6.4 Hz, 3H), 3.39 (t, J = 6.8 Hz, 2H), 2.90−2.86 (m, 1H), 2.62−2.50 (m, 2H), 2.08−2.02 (m, 1H), 1.78−1.72 (m, 2H), 1.48−1.29 (m, 8H); ^{13}C NMR (100 MHz, DMSO-d_6) δ (ppm) 173.24, 170.42, 167.32, 165.77, 156.50, 137.47, 133.72, 120.23, 116.69, 115.57, 69.27, 61.16, 49.22, 32.94, 31.43, 29.07, 28.89, 25.94, 25.82, 22.48. UPLC−MS calculated for $C_{20}H_{25}N_2O_6$ $[M + H]^+$: 389.17, found 389.18.

MsCl (0.14 mL, 1.70 mmol, 1.2 equiv) and TEA (0.30 mL, 2.13 mmol, 1.5 equiv) were added sequentially to a solution of compound **46** (589 mg, 1.42 mmol, 1.0 equiv) in DCM (10 mL) at 0 °C. The resulting solution was stirred at 0 °C for 2 h. Then the solvent was evaporated to afford the crude residue. Sodium azide (277 mg, 4.25 mmol, 3.0 equiv) was added to the above residue in DMF (6 mL). The solution was stirred at 70 °C for 2 h and then filtered through Celite. The residue was purified by preparative HPLC to afford the desired product as a white solid (386 mg, 66% yield in two steps). 10% Pd/C (30 mg) was added to the above compound in EtOH (10 mL). The flask was purged and refilled with H_2 three times. The solution was stirred at room temperature under H_2 for 12 h. Filtration through Celite removed the Pd/C, and then the solution was concentrated and the residue was purified by preparative HPLC to afford the desired compound **47** as a colorless oil (72 mg, 20% yield).

HATU (27 mg, 0.07 mmol, 1.4 equiv), DIPEA (27 μL, 0.15 mmol, 3.0 equiv), and the amine **47** (27.1 mg, 0.07 mmol, 1.4 equiv) were added sequentially to a stirred solution of the intermediate **34** (24 mg, 0.05 mmol, 1.0 equiv) in DMF (2.0 mL). The solution was stirred at room temperature for 2 h. Preparative HPLC purification afforded the pure product **11** as a slightly yellow solid (19 mg, 45% yield). ^{1}H NMR (400 MHz, DMSO-d_6) δ (ppm) 12.30 (s, 1H), 11.08 (s, 1H), 9.28 (s, 1H), 8.16 (t, J = 5.6 Hz, 1H), 7.79 (t, J = 8.0 Hz, 1H), 7.52 (s, 1H), 7.51 (d, J = 8.0 Hz, 1H), 7.43 (d, J = 8.0 Hz, 1H), 7.34 (s, 1H), 5.94 (s, 1H), 5.07 (dd, J = 12.8 Hz, J = 5.6 Hz, 1H), 4.21 (t, J = 6.4 Hz, 1H), 3.94 (q, J = 7.2 Hz, 2H), 3.83 (s, 3H), 3.29−3.24 (m, 2H), 2.91−2.82 (m, 1H), 2.59−2.44 (m, 2H), 2.30 (s, 3H), 2.10 (s, 3H), 2.05−1.99 (m, 1H), 1.91−1.84 (m, 1H), 1.81−1.74 (m, 2H), 1.53−1.47 (m, 4H), 1.41−1.30 (m, 7H), 0.86−0.81 (m, 2H), 0.64−0.60 (m, 2H). UPLC−MS calculated for $C_{45}H_{49}N_{10}O_8$ $[M + H]^+$: 857.37, found 857.35. Purity, 98.2%.

General Procedure for Synthesis of Compounds 12−17. In a round-bottom flask, 3-fluorophthalic anhydride **48** (6.64 g, 40 mmol, 1.0 equiv), 3-aminopiperidine-2,6-dione hydrochloride **38** (6.58 g, 40 mmol, 1.0 equiv), and sodium acetate (3.94 g, 48 mmol, 1.2 equiv) were mixed in AcOH (120 mL). The resulting reaction mixture was heated to reflux at 140 °C for 12 h. After cooling to room temperature, most of the AcOH was evaporated and the residue was purified by flash column chromatography with DCM/MeOH to obtain compound **49** as a slightly yellow solid (9.7 g, 88% yield). UPLC−MS calculated for $C_{13}H_{10}FN_2O_4$ $[M + H]^+$: 277.06, found 277.02. ^{1}H NMR (400 MHz, DMSO-d_6) δ (ppm) 11.15 (s, 1H), 7.98−7.93 (m, 1H), 7.80−7.72 (m, 2H), 5.17 (dd, J = 13.2 Hz, J = 5.2 Hz, 1H), 2.95−2.86 (m, 1H), 2.64−2.47 (m, 2H), 2.10−2.06 (m, 1H).

Mono-Boc protected alkyl diamines (1.13 mmol, 1.1 equiv) of different lengths were added to a stirred solution of compound **49** (285 mg, 1.03 mmol, 1.0 equiv) in DMF (6.0 mL) and DIPEA (0.36 mL, 2.06 mmol, 2.0 equiv). The reaction mixture was stirred at 90 °C for 12 h. Then the mixture was cooled to room temperature, poured into H_2O, and extracted twice with EtOAc. The combined organic layer was washed with brine, dried over anhydrous Na_2SO_4. After filtration and evaporation, the crude residue was purified by preparative HPLC to give the intermediate (**50a−f**) which was dissolved in DCM (4.0 mL) and TFA (2.0 mL). After stirring for 1 h, the solvent was evaporated to give the crude product **51a−f**, which was used in the next step without further purification.

HATU (27 mg, 0.07 mmol, 1.4 equiv), DIPEA (27 μL, 0.15 mmol, 3.0 equiv), and the amine intermediate **51a−f** (0.07 mmol, 1.4 equiv) were added sequentially to a stirred solution of compound **34** (24 mg,

DOI: 10.1021/acs.jmedchem.6b01816
J. Med. Chem. 2018, 61, 462−481

0.05 mmol, 1.0 equiv) in DMF (2.0 mL). The solution was stirred at room temperature for 2 h. Preparative HPLC purification afforded the pure product **12**–**17**.

4-((3-Cyclopropyl-1-ethyl-1*H*-pyrazol-5-yl)amino)-7-(3,5-dimethylisoxazol-4-yl)-*N*-(7-((2-(2,6-dioxopiperidin-3-yl)-1,3-dioxoisoindolin-4-yl)amino)heptyl)-6-methoxy-9*H*-pyrimido-[4,5-*b*]indole-2-carboxamide (12). ^{1}H NMR (400 MHz, DMSO-d_6) δ (ppm) 12.30 (s, 1H), 11.08 (s, 1H), 9.31 (s, 1H), 8.17 (s, 1H), 7.58–7.54 (m, 2H), 7.39 (s, 1H), 7.08 (d, J = 8.4 Hz, 1H), 7.00 (d, J = 6.8 Hz, 1H), 6.52 (s, 1H), 5.95 (s, 1H), 5.04 (dd, J = 12.8 Hz, J = 5.6 Hz, 1H), 3.95 (q, J = 7.2 Hz, 2H), 3.83 (s, 3H), 3.31–3.25 (m, 4H), 2.92–2.83 (m, 1H), 2.59–2.49 (m, 2H), 2.30 (s, 3H), 2.10 (s, 3H), 2.05–2.00 (m, 1H), 1.90–1.85 (m, 1H), 1.61–1.56 (m, 2H), 1.54–1.49 (m, 2H), 1.45–1.28 (m, 6H), 1.30 (t, J = 7.2 Hz, 3H), 0.87–0.82 (m, 2H), 0.65–0.61 (m, 2H). UPLC–MS calculated for $C_{45}H_{50}N_{11}O_7$ $[M + H]^+$: 856.39, found 856.39. Purity, 97.9%.

4-((3-Cyclopropyl-1-ethyl-1*H*-pyrazol-5-yl)amino)-7-(3,5-dimethylisoxazol-4-yl)-*N*-(6-((2-(2,6-dioxopiperidin-3-yl)-1,3-dioxoisoindolin-4-yl)amino)hexyl)-6-methoxy-9*H*-pyrimido[4,5-*b*]indole-2-carboxamide (13). ^{1}H NMR (400 MHz, methanol-d_4) δ 7.54 (s, 1H), 7.46 (s, 1H), 7.39–7.36 (m, 1H), 7.02 (d, J = 7.4 Hz, 1H), 6.93 (d, J = 7.1 Hz, 1H), 5.49 (s, 1H), 5.05–4.98 (m, 1H), 4.24–4.17 (q, J = 7.3 Hz, 2H), 3.98 (s, 2H), 3.89 (s, 3H), 3.37–3.22 (m, 6H), 3.00 (s, 2H), 2.88–2.84 (m, 2H), 2.68–2.64 (m, 2H), 2.34 (s, 3H), 2.17 (s, 3H), 1.98–1.91 (m, 1H), 1.73–1.68 (m, 2H), 1.48 (t, J = 7.3 Hz, 3H), 1.15–1.05 (m, 2H), 0.89–0.81 (m, 2H). UPLC–MS calculated for $C_{44}H_{47}N_{11}O_7$ $[M + H]^+$: 842.37, found 842.36. UPLC analysis (10 min from 10% to 100% (MeCN/H_2O containing 0.1% CF_3CO_2H)): retention time, 5.21 min; peak area, 98.5%.

4-((3-Cyclopropyl-1-ethyl-1*H*-pyrazol-5-yl)amino)-7-(3,5-dimethylisoxazol-4-yl)-*N*-(5-((2-(2,6-dioxopiperidin-3-yl)-1,3-dioxoisoindolin-4-yl)amino)pentyl)-6-methoxy-9*H*-pyrimido-[4,5-*b*]indole-2-carboxamide (14). ^{1}H NMR (400 MHz, MeOD-d_4) δ 7.51–7.42 (m, 2H), 7.38 (s, 1H), 6.98 (d, J = 8.9 Hz, 1H), 6.88 (d, J = 7.0 Hz, 1H), 6.08 (s, 1H), 4.93–4.97 (m, 1H), 4.15 (q, J = 7.0 Hz, 2H), 3.88 (s, 3H), 3.52–3.48 (m, 2H), 3.35 (s, 4H), 2.74–2.53 (m, 2H), 2.34 (s, 3H), 2.17 (s, 3H), 2.05–1.93 (m, 4H), 1.78–1.64 (m, 2H), 1.42 (t, J = 7.0 Hz, 3H), 1.40–1.34 (m, 1H), 1.08–0.96 (m, 2H), 0.80–0.73 (m, 2H). UPLC–MS calculated for $C_{43}H_{45}N_{11}O_7$ $[M + H]^+$: 828.35, found 828.35. UPLC analysis (10 min from 10% to 100% (MeCN/H_2O containing 0.1% CF_3CO_2H)): retention time, 4.80 min; peak area, 99.4%.

4-((3-Cyclopropyl-1-ethyl-1*H*-pyrazol-5-yl)amino)-7-(3,5-dimethylisoxazol-4-yl)-*N*-(4-((2-(2,6-dioxopiperidin-3-yl)-1,3-dioxoisoindolin-4-yl)amino)butyl)-6-methoxy-9*H*-pyrimido[4,5-*b*]indole-2-carboxamide (15). ^{1}H NMR (400 MHz, DMSO-d_6) δ (ppm) 12.29 (s, 1H), 11.08 (s, 1H), 9.36 (s, 1H), 8.31 (t, J = 5.6 Hz, 1H), 7.56 (t, J = 7.2 Hz, 1H), 7.49 (s, 1H), 7.40 (s, 1H), 7.12 (d, J = 8.4 Hz, 1H), 7.01 (d, J = 6.8 Hz, 1H), 6.58 (s, 1H), 5.96 (s, 1H), 5.05 (dd, J = 12.8 Hz, J = 5.2 Hz, 1H), 3.97 (q, J = 7.2 Hz, 2H), 3.83 (s, 3H), 3.40–3.30 (m, 4H), 2.92–2.83 (m, 1H), 2.60–2.49 (m, 2H), 2.30 (s, 3H), 2.10 (s, 3H), 2.07–2.01 (m, 1H), 1.91–1.84 (m, 1H), 1.65–1.55 (m, 4H), 1.31 (t, J = 7.2 Hz, 3H), 0.86–0.81 (m, 2H), 0.64–0.60 (m, 2H). UPLC–MS calculated for $C_{42}H_{44}N_{11}O_7$ $[M + H]^+$: 814.34, found 814.37. Purity, 89.9%.

4-((3-Cyclopropyl-1-ethyl-1*H*-pyrazol-5-yl)amino)-7-(3,5-dimethylisoxazol-4-yl)-*N*-(3-((2-(2,6-dioxopiperidin-3-yl)-1,3-dioxoisoindolin-4-yl)amino)propyl)-6-methoxy-9*H*-pyrimido-[4,5-*b*]indole-2-carboxamide (16). ^{1}H NMR (400 MHz, MeOD-d_4) δ 7.55–7.49 (m, 2H), 7.39 (s, 1H), 7.04 (d, J = 8.8 Hz, 1H), 6.98 (d, J = 7.1 Hz, 1H), 4.89–4.81 (m, 1H), 4.18 (q, J = 7.3 Hz, 2H), 3.89 (s, 3H), 3.70–3.56 (m, 2H), 3.52–3.42 (m, 2H), 3.35 (d, J = 1.4 Hz, 2H), 2.34 (s, 3H), 2.17 (s, 3H), 2.05–2.01 (m, 4H), 1.88–1.79 (m, 1H), 1.44 (t, J = 7.3 Hz, 3H), 1.09–1.01 (m, 2H), 0.82–0.73 (m, 2H). UPLC–MS calculated for $C_{41}H_{41}N_{11}O_7$ $[M + H]^+$: 800.32, found 800.23. UPLC analysis (10 min from 10% to 100% (MeCN/H_2O containing 0.1% CF_3CO_2H)): retention time, 4.43 min; peak area, 98.0%.

4-((3-Cyclopropyl-1-ethyl-1*H*-pyrazol-5-yl)amino)-7-(3,5-dimethylisoxazol-4-yl)-*N*-(2-((2-(2,6-dioxopiperidin-3-yl)-1,3-dioxoisoindolin-4-yl)amino)ethyl)-6-methoxy-9*H*-pyrimido[4,5-*b*]indole-2-carboxamide (17). ^{1}H NMR (400 MHz, methanol-d_4) δ 7.55–7.48 (m, 1H), 7.46 (s, 1H), 7.33–7.27 (m, 1H), 7.20 (d, J = 8.6 Hz, 1H), 7.01 (d, J = 7.1 Hz, 1H), 6.16 (s, 1H), 5.05–4.95 (m, 1H), 4.20 (q, J = 7.2 Hz, 2H), 3.87 (s, 3H), 3.72–3.70 (m, 2H), 3.66–3.62 (m, 2H), 2.83–2.73 (m, 1H), 2.71–2.58 (m, 2H), 2.33 (s, 3H), 2.16 (s, 3H), 1.99–1.97 (m, 1H), 1.46 (t, J = 7.2 Hz, 3H), 1.11–1.02 (m, 2H), 0.83–0.79 (m, 2H). UPLC–MS (ESI^+): m/z calculated for $C_{40}H_{39}N_{11}O_7$ $[M + H]^+$: 786.30, found 786.18. UPLC analysis (10 min from 10% to 100% (MeCN/H_2O containing 0.1% CF_3CO_2H)): retention time, 4.37 min; peak area, 97.4%.

4-((3-Cyclopropyl-1-ethyl-1*H*-pyrazol-5-yl)amino)-7-(3,5-dimethylisoxazol-4-yl)-*N*-(6-(2-(2,6-dioxopiperidin-3-yl)-1,3-dioxoisoindolin-4-yl)hexyl)-6-methoxy-9*H*-pyrimido[4,5-*b*]-indole-2-carboxamide (18). In a round-bottom flask, 3-bromophthalic anhydride **52** (2.27 g, 10.0 mmol, 1.0 equiv), 3-aminopiperidine-2,6-dione hydrochloride **38** (1.81 g, 11 mmol, 1.1 equiv), and sodium acetate (0.98 g, 12 mmol, 1.2 equiv) were mixed in acetic acid (30 mL). The resulting reaction mixture was heated to reflux at 140 °C for 12 h. After cooling to room temperature, most of the AcOH was evaporated and the residue was purified by flash column chromatography with DCM/MeOH to give compound **53** as a purple solid (2.70 g, 80% yield). ^{1}H NMR (400 MHz, DMSO-d_6) δ 11.15 (s, 1H), 8.06 (d, J = 8.0 Hz, 1H), 7.94 (d, J = 7.2 Hz, 1H), 7.78 (t, J = 7.6 Hz, 1H), 5.18 (dd, J = 12.8 Hz, J = 5.6 Hz, 1H), 2.95–2.86 (m, 1H), 2.65–2.48 (m, 2H), 2.11–2.05 (m, 1H); ^{13}C NMR (100 MHz, DMSO-d_6) δ 173.21, 170.18, 166.07, 165.65, 139.66, 136.73, 134.15, 129.20, 123.31, 118.11, 49.65, 31.39, 22.30. UPLC–MS calculated for $C_{13}H_{10}BrN_2O_4$ $[M + H]^+$: 336.98, found 336.95.

In a round-bottom flask, compound **53** (674 mg, 2.0 mmol, 1.0 equiv) and *tert*-butyl hex-5-yn-1-ylcarbamate (934 mg, 4.0 mmol, 2.0 equiv) were added to a solution of CuI (76 mg, 0.4 mmol, 0.2 equiv) and $Pd(PPh_3)_2Cl_2$ (140 mg, 0.2 mmol, 0.1 equiv) in DMF (10 mL). The solution was purged and refilled with nitrogen three times. Then trimethylamine (5.0 mL) was added. The solution was purged and refilled with nitrogen again. The mixture was stirred at 70 °C for 3 h under Ar. The solution was cooled to room temperature and filtered through Celite. The residue was purified by flash column chromatography to yield compound **54b** as a slightly yellow solid (653 mg, 72% yield). UPLC–MS calculated for $C_{24}H_{27}N_3NaO_6$ $[M + Na]^+$ = 476.18, found 476.18.

10% Pd/C (60 mg) was added to a solution of compound **54b** (653 mg, 1.44 mmol, 1.0 equiv) in EtOH (10 mL) under N_2. The solution was purged and refilled with hydrogen three times. The solution was stirred at room temperature for 12 h. After filtration, the solvent was evaporated to give the crude residue **55b**, which was dissolved in DCM (4.0 mL) and TFA (2.0 mL). The reaction mixture was stirred at room temperature for 1 h. Preparative HPLC purification afforded compound **56b** as a colorless oil (411 mg, 80% yield in two steps).

HATU (27 mg, 0.07 mmol, 1.4 equiv), DIPEA (27 μL, 0.15 mmol, 3.0 equiv), and **56b** (25 mg, 0.07 mmol, 1.4 equiv) were added sequentially to a stirred solution of compound **34** (24 mg, 0.05 mmol, 1.0 equiv) in DMF (2.0 mL). The solution was stirred at room temperature for 2 h. Preparative HPLC purification afforded the pure product **18** as a slightly yellow solid (29 mg, 70% yield). ^{1}H NMR (400 MHz, DMSO-d_6) δ (ppm) 12.25 (s, 1H), 11.10 (s, 1H), 9.29 (s, 1H), 8.15 (t, J = 5.6 Hz, 1H), 7.78–7.69 (m, 3H), 7.58 (s, 1H), 7.37 (s, 1H), 5.94 (s, 1H), 5.12 (dd, J = 13.2 Hz, J = 5.2 Hz, 1H), 3.94 (q, J = 7.2 Hz, 2H), 3.83 (s, 3H), 3.28–3.23 (m, 2H), 3.05 (t, J = 8.0 Hz, 2H), 2.93–2.83 (m, 1H), 2.61–2.49 (m, 2H), 2.30 (s, 3H), 2.10 (s, 3H), 2.07–2.03 (m, 1H), 1.89–1.82 (m, 1H), 1.66–1.60 (m, 2H), 1.53–1.47 (m, 2H), 1.36–1.27 (m, 7H), 0.84–0.79 (m, 2H), 0.63–0.59 (m, 2H). UPLC–MS calculated for $C_{44}H_{47}N_{10}O_7$ $[M + H]^+$: 827.36, found 827.28. Purity, 98.7%.

4-((3-Cyclopropyl-1-ethyl-1*H*-pyrazol-5-yl)amino)-7-(3,5-dimethylisoxazol-4-yl)-*N*-(2-(3-(2-(2,6-dioxopiperidin-3-yl)-1,3-dioxoisoindolin-4-yl)propoxy)ethyl)-6-methoxy-9*H*-pyrimido-[4,5-*b*]indole-2-carboxamide (19). Following the procedure for the synthesis of compound **18** from the intermediate **53**, compound **19** was obtained with *tert*-butyl (2-(prop-2-yn-1-yloxy)ethyl)carbamate as the linker instead of *t*-butyl hex-5-yn-1-ylcarbamate. ^{1}H NMR (400 MHz, DMSO-d_6) δ (ppm) 12.24 (s, 1H), 11.10 (s, 1H), 9.27 (s, 1H),

DOI: 10.1021/acs.jmedchem.6b01816
J. Med. Chem. 2018, 61, 462–481

8.23 (t, J = 5.6 Hz, 1H), 7.73−7.68 (m, 3H), 7.57 (s, 1H), 7.35 (s, 1H), 5.91 (s, 1H), 5.11 (dd, J = 12.8 Hz, J = 5.2 Hz, 1H), 3.94 (q, J = 7.2 Hz, 2H), 3.83 (s, 3H), 3.50−3.43 (m, 6H), 3.09 (t, J = 7.6 Hz, 2H), 2.92−2.82 (m, 1H), 2.61−2.46 (m, 2H), 2.30 (s, 3H), 2.10 (s, 3H), 2.05−2.02 (m, 2H), 1.93−1.82 (m, 3H), 1.29 (t, J = 7.2 Hz, 3H), 0.84−0.79 (m, 2H), 0.63−0.59 (m, 2H). UPLC−MS calculated for $C_{43}H_{45}N_{10}O_8$ $[M + H]^+$: 829.34, found 829.41. Purity, >99.0%.

4-((3-Cyclopropyl-1-ethyl-1*H*-pyrazol-5-yl)amino)-7-(3,5-dimethylisoxazol-4-yl)-*N*-(5-(2-(2,6-dioxopiperidin-3-yl)-1,3-dioxoisoindolin-4-yl)pentyl)-6-methoxy-9*H*-pyrimido[4,5-*b*]indole-2-carboxamide (20). Following the procedure used in the synthesis of compound **18** from the intermediate **53**, compound **20** was obtained with *tert*-butyl pent-4-yn-1-ylcarbamate as the linker instead of *tert*-butyl hex-5-yn-1-ylcarbamate. ^{1}H NMR (400 MHz, DMSO-d_6) δ (ppm) 12.22 (s, 1H), 11.10 (s, 1H), 9.29 (s, 1H), 8.19 (t, J = 5.6 Hz, 1H), 7.76−7.71 (m, 3H), 7.54 (s, 1H), 7.35 (s, 1H), 5.93 (s, 1H), 5.12 (dd, J = 13.2 Hz, J = 5.2 Hz, 1H), 3.95 (q, J = 7.2 Hz, 2H), 3.82 (s, 3H), 3.29−3.24 (m, 2H), 3.06 (t, J = 8.0 Hz, 2H), 2.92−2.83 (m, 1H), 2.61−2.55 (m, 2H), 2.30 (s, 3H), 2.10 (s, 3H), 2.05−2.00 (m, 1H), 1.90−1.85 (m, 1H), 1.67−1.61 (m, 2H), 1.57−1.52 (m, 2H), 1.41−1.35 (m, 2H), 1.31 (t, J = 7.2 Hz, 3H), 0.85−0.81 (m, 2H), 0.63−0.59 (m, 2H). UPLC−MS calculated for $C_{43}H_{44}N_{10}O_7$ $[M + H]^+$: 812.34, found 813.33. Purity, 95.3%.

General Procedure for Synthesis of Compounds 21−25 and 27. NBS (17.09 g, 96 mmol, 1.2 equiv) and BPO (1.938 g, 8.0 mmol, 0.1 equiv) were added to a stirred solution of methyl 3-bromo-2-methylbenzoate **57** (18.33 g, 80 mmol, 1.0 equiv) in benzene (150 mL). The solution was heated at reflux for 6 h. After cooling to room temperature, the solvent was evaporated and the residue was purified by flash column chromatography with hexane/EtOAc to afford the intermediate **58** (22.17 g, 90% yield) as a slightly yellow solid.

Compound **38** (14.48 g, 88 mmol, 1.22 equiv) and TEA (13.38 mL, 96 mmol, 1.33 equiv) were added to a stirred solution of compound **58** (22.17 g, 72 mmol, 1.0 equiv) in MeCN (150 mL). The solution was stirred at 80 °C for 12 h and then cooled to room temperature, and most of the solvent was evaporated. EtOAc (200 mL) and H_2O (200 mL) were added to the residue and the solution was filtered to afford the crude product as a purple solid **59** (17.4 g, 75% yield). ^{1}H NMR (400 MHz, DMSO-d_6) δ (ppm) 11.00 (s, 1H), 7.87 (d, J = 7.6 Hz, 1H), 7.77 (d, J = 7.6 Hz, 1H), 7.51 (t, J = 8.0 Hz, 1H), 5.15 (dd, J = 13.2 Hz, J = 5.2 Hz, 1H), 4.42 (d, J = 17.6 Hz, 1H), 4.27 (d, J = 17.6 Hz, 1H), 2.96−2.87 (m, 1H), 2.62−2.42 (m, 2H), 2.07−2.00 (m, 1H); ^{13}C NMR (100 MHz, DMSO-d_6) δ (ppm) 173.30, 171.32, 167.69, 142.58, 135.10, 134.41, 130.98, 122.96, 117.79, 52.22, 48.46, 31.66, 22.74. UPLC−MS calculated for $C_{13}H_{12}BrN_2O_3$ $[M + H]^+$: 323.00, found 322.90.

Following the procedures used to prepare compound **18** from the intermediate **53**, compounds **21−25** and **27** with different alkynyl chains were obtained as indicated in Schemes 8 and 9.

4-((3-Cyclopropyl-1-ethyl-1*H*-pyrazol-5-yl)amino)-7-(3,5-dimethylisoxazol-4-yl)-*N*-(6-(2-(2,6-dioxopiperidin-3-yl)-1-oxoisoindolin-4-yl)hexyl)-6-methoxy-9*H*-pyrimido[4,5-*b*]indole-2-carboxamide (21). ^{1}H NMR (400 MHz, DMSO-d_6) δ (ppm) 12.25 (s, 1H), 10.97 (s, 1H), 9.31 (s, 1H), 8.16 (t, J = 5.2 Hz, 1H), 7.60−7.21 (m, 5H), 5.95 (s, 1H), 5.13 (dd, J = 13.2 Hz, J = 4.8 Hz, 1H), 4.48 (d, J = 17.2 Hz, 1H), 4.32 (d, J = 17.2 Hz, 1H), 3.95 (q, J = 7.2 Hz, 2H), 3.83 (s, 3H), 3.29−3.24 (m, 2H), 2.94−2.87 (m, 1H), 2.73−2.45 (m, 4H), 2.30 (s, 3H), 2.10 (s, 3H), 2.03−1.98 (m, 1H), 1.89−1.82 (m, 1H), 1.66−1.62 (m, 2H), 1.52−1.48 (m, 2H), 1.36−1.27 (m, 7H), 0.84−0.79 (m, 2H), 0.63−0.59 (m, 2H). UPLC−MS calculated for $C_{44}H_{49}N_{10}O_6$ $[M + H]^+$: 813.38, found 813.29. Purity, 95.3%.

4-((3-Cyclopropyl-1-ethyl-1*H*-pyrazol-5-yl)amino)-7-(3,5-dimethylisoxazol-4-yl)-*N*-(2-(3-(2-(2,6-dioxopiperidin-3-yl)-1-oxoisoindolin-4-yl)propoxy)ethyl)-6-methoxy-9*H*-pyrimido[4,5-*b*]indole-2-carboxamide (22). ^{1}H NMR (400 MHz, DMSO-d_6) δ (ppm) 12.23 (s, 1H), 10.96 (s, 1H), 9.27 (s, 1H), 8.23 (t, J = 5.2 Hz, 1H), 7.57−7.41 (m, 4H), 7.35 (s, 1H), 5.90 (s, 1H), 5.10 (dd, J = 13.2 Hz, J = 5.2 Hz, 1H), 4.47 (d, J = 17.2 Hz, 1H), 4.32 (d, J = 17.2 Hz, 1H), 3.93 (q, J = 7.2 Hz, 2H), 3.83 (s, 3H), 3.50−3.40 (m, 6H), 2.88−2.84 (m, 1H), 2.71 (t, J = 7.6 Hz, 2H), 2.67−2.43 (m, 2H), 2.30 (s, 3H), 2.10 (s, 3H), 1.98−1.81 (m, 4H), 1.29 (t, J = 7.2 Hz, 3H), 0.83−0.78 (m, 2H), 0.62−0.58 (m, 2H). UPLC−MS calculated for $C_{43}H_{47}N_{10}O_7$ $[M + H]^+$: 815.36, found 815.26. Purity, >99.0%.

4-((3-Cyclopropyl-1-ethyl-1*H*-pyrazol-5-yl)amino)-7-(3,5-dimethylisoxazol-4-yl)-*N*-(5-(2-(2,6-dioxopiperidin-3-yl)-1-oxoisoindolin-4-yl)pentyl)-6-methoxy-9*H*-pyrimido[4,5-*b*]indole-2-carboxamide (23). See Figures S2−S4 in Supporting Information. ^{1}H NMR (400 MHz, DMSO-d_6) δ (ppm) 12.21 (s, 1H), 10.98 (s, 1H), 9.29 (s, 1H), 8.18 (t, J = 5.2 Hz, 1H), 7.57 (d, J = 6.8 Hz, 2H), 7.49−7.43 (m, 2H), 7.35 (s, 1H), 5.93 (s, 1H), 5.13 (dd, J = 13.2 Hz, J = 5.2 Hz, 1H), 4.49 (d, J = 17.2 Hz, 1H), 4.33 (d, J = 17.2 Hz, 1H), 3.95 (q, J = 7.2 Hz, 2H), 3.83 (s, 3H), 3.29−3.24 (m, 2H), 2.96−2.87 (m, 1H), 2.70−2.44 (m, 4H), 2.30 (s, 3H), 2.10 (s, 3H), 2.03−2.00 (m, 1H), 1.88−1.85 (m, 1H), 1.67−1.65 (m, 2H), 1.58−1.54 (m, 2H), 1.39−1.24 (m, 5H), 0.84−0.82 (m, 2H), 0.63−0.59 (m, 2H); ^{13}C NMR (100 MHz, DMSO-d_6) δ (ppm) 172.87, 171.04, 168.37, 165.48, 162.96, 159.17, 156.48, 155.10, 154.07, 152.42, 152.20, 140.49, 137.46, 136.47, 131.88, 131.56, 131.43, 128.26, 120.60, 119.04, 117.43, 113.85, 113.41, 104.51, 98.35, 97.22, 56.01, 51.55, 46.24, 42.41, 31.16, 29.00, 28.80, 26.30, 22.51, 14.86, 11.28, 10.34, 9.58, 7.59. UPLC−MS calculated for $C_{43}H_{47}N_{10}O_6$ $[M + H]^+$: 799.37, found 799.19. Purity, 98.9%.

4-((3-Cyclopropyl-1-ethyl-1*H*-pyrazol-5-yl)amino)-7-(3,5-dimethylisoxazol-4-yl)-*N*-(4-(2-(2,6-dioxopiperidin-3-yl)-1-oxoisoindolin-4-yl)butyl)-6-methoxy-9*H*-pyrimido[4,5-*b*]indole-2-carboxamide (24). ^{1}H NMR (400 MHz, DMSO-d_6) δ (ppm) 12.22 (s, 1H), 10.96 (s, 1H), 9.29 (s, 1H), 8.23 (t, J = 6.0 Hz, 1H), 7.58−7.44 (m, 4H), 7.36 (s, 1H), 5.92 (s, 1H), 5.11 (dd, J = 13.2 Hz, J = 5.2 Hz, 1H), 4.47 (d, J = 17.2 Hz, 1H), 4.32 (d, J = 17.2 Hz, 1H), 3.94 (q, J = 7.2 Hz, 2H), 3.83 (s, 3H), 3.35−3.32 (m, 2H), 2.94−2.84 (m, 1H), 2.69 (t, J = 7.6 Hz, 2H), 2.56−2.35 (m, 2H), 2.30 (s, 3H), 2.10 (s, 3H), 2.01−1.96 (m, 1H), 1.87−1.80 (m, 1H), 1.67−1.54 (m, 4H), 1.29 (t, J = 7.2 Hz, 3H), 0.84−0.79 (m, 2H), 0.62−0.58 (m, 2H). UPLC−MS calculated for $C_{42}H_{45}N_{10}O_6$ $[M + H]^+$: 785.35, found 785.32. Purity, 94.2%.

4-((3-Cyclopropyl-1-ethyl-1*H*-pyrazol-5-yl)amino)-7-(3,5-dimethylisoxazol-4-yl)-*N*-(3-(2-(2,6-dioxopiperidin-3-yl)-1-oxoisoindolin-4-yl)propyl)-6-methoxy-9*H*-pyrimido[4,5-*b*]indole-2-carboxamide (25). ^{1}H NMR (400 MHz, MeOD-d_4) δ (ppm) 7.59 (d, J = 7.2 Hz, 1H), 7.50−7.43 (m, 3H), 7.25 (s, 1H), 5.98 (s, 1H), 5.09 (dd, J = 13.2 Hz, J = 4.8 Hz, 1H), 4.48 (d, J = 17.2 Hz, 1H), 4.42 (d, J = 17.2 Hz, 1H), 4.13 (q, J = 6.8 Hz, 2H), 3.86 (s, 3H), 3.50−3.40 (m, 2H), 2.83−2.61 (m, 4H), 2.45−2.25 (m, 4H), 2.25−1.91 (m, 7H), 1.43 (t, J = 7.2 Hz, 3H), 0.92−0.89 (m, 2H), 0.68−0.66 (m, 2H). UPLC−MS calculated for $C_{41}H_{43}N_{10}O_6$ $[M + H]^+$: 771.34, found 771.35. Purity, >99.0%.

4-((3-Cyclopropyl-1-ethyl-1*H*-pyrazol-5-yl)amino)-7-(3,5-dimethylisoxazol-4-yl)-6-methoxy-*N*-(5-(2-(1-methyl-2,6-dioxopiperidin-3-yl)-1-oxoisoindolin-4-yl)pentyl)-9*H*-pyrimido[4,5-*b*]indole-2-carboxamide (26). K_2CO_3 (332 mg, 2.4 mmol, 1.2 equiv) and MeI (0.19 mL, 3.0 mmol, 1.5 equiv) were added to a solution of compound **59** (646 mg, 2.0 mmol, 1.0 equiv) in DMF (5.0 mL). The solution was stirred at 60 °C for 3 h. Preparative HPLC purification afforded the desired compound **63** as a white solid (485 mg, 72% yield). ^{1}H NMR (400 MHz, DMSO-d_6) δ (ppm) 7.86 (d, J = 8.4 Hz, 1H), 7.78 (d, J = 7.2 Hz, 1H), 7.51 (t, J = 7.6 Hz, 1H), 5.22 (dd, J = 13.2 Hz, J = 5.2 Hz, 1H), 4.41 (d, J = 17.6 Hz, 1H), 4.26 (d, J = 17.6 Hz, 1H), 3.06−2.95 (m, 4H), 2.79−2.73 (m, 1H), 2.52−2.41 (m, 1H), 2.07−2.01 (m, 1H); ^{13}C NMR (100 MHz, DMSO-d_6) δ (ppm) 172.33, 170.94, 167.73, 142.60, 135.11, 134.38, 130.96, 122.99, 117.79, 52.69, 48.41, 31.80, 27.06, 22.05. UPLC−MS calculated for $C_{14}H_{14}BrN_2O_3$ $[M + H]^+$: 337.02, found 336.98.

Following the procedures used for the conversion of the intermediates **53−18**, compound **26** was obtained from the intermediate **63**. ^{1}H NMR (400 MHz, MeOD-d_4) δ (ppm) 7.56−7.54 (m, 2H), 7.43−7.36 (m, 3H), 6.20 (s, 1H), 5.12 (dd, J = 13.6 Hz, J = 5.2 Hz, 1H), 4.47 (d, J = 17.2 Hz, 1H), 4.41 (d, J = 17.2 Hz, 1H), 4.22 (q, J = 6.8 Hz, 2H), 3.89 (s, 3H), 3.50−3.40 (m, 2H), 3.07 (s, 3H), 2.90−2.81 (m, 2H), 2.72−2.61 (m, 2H), 2.51−2.40 (m, 1H), 2.32 (s, 3H), 2.16 (s, 3H), 2.13−2.09 (m, 1H), 2.03−1.99 (m, 1H), 1.70−1.66 (m, 4H), 1.48−1.44 (m, 5H), 1.10−1.05 (m, 2H), 0.83−

DOI: 10.1021/acs.jmedchem.6b01816
J. Med. Chem. 2018, 61, 462−481

0.81 (m, 2H). UPLC−MS calculated for $C_{44}H_{49}N_{10}O_6$ $[M + H]^+$: 813.38, found 813.34. Purity, >99.0%.

7-(3,5-Dimethylisoxazol-4-yl)-*N*-(5-(2-(2,6-dioxopiperidin-3-yl)-1-oxoisoindolin-4-yl)pentyl)-6-methoxy-9*H*-pyrimido[4,5-*b*]indole-2-carboxamide (27). ^{1}H NMR (400 MHz, DMSO-d_6) δ (ppm) 12.57 (s, 1H), 10.97 (s, 1H), 9.60 (s, 1H), 9.01 (t, J = 6.0 Hz, 1H), 8.12 (s, 1H), 7.56−7.54 (m, 2H), 7.52 (s, 1H), 7.48−7.41 (m, 2H), 5.13 (dd, J = 13.2 Hz, J = 5.2 Hz, 1H), 4.48 (d, J = 17.2 Hz, 1H), 4.32 (d, J = 17.2 Hz, 1H), 3.91 (s, 3H), 3.38−3.33 (m, 2H), 2.96−2.87 (m, 1H), 2.68−2.57 (m, 3H), 2.51−2.42 (m, 1H), 2.32 (s, 3H), 2.12 (s, 3H), 2.07−1.99 (m, 1H), 1.69−1.60 (m, 4H), 1.44−1.36 (m, 2H). UPLC−MS calculated for $C_{35}H_{36}N_7O_6$ $[M + H]^+$: 650.27, found 650.26. Purity, >99.0%.

7-(3,5-Dimethylisoxazol-4-yl)-6-methoxy-*N*-methyl-9*H*-pyrimido[4,5-*b*]indole-2-carboxamide (28). 10% Pd/C (20 mg) was added to a stirred solution of compound **33** (200 mg, 0.52 mmol, 1.0 equiv) in 10 mL of DMF under N_2. The flask was purged and refilled with H_2 three times. The solution was then stirred at 60 °C for 12 h. After cooling to room temperature, the solution was filtered through Celite. After concentration, the residue crude intermediate **35** was suspended in THF (30 mL), and LiOH (38 mg, 1.55 mmol, 3.0 equiv) was added. The resulting solution was stirred at room temperature for 12 h. After concentration, the residue was purified by preparative HPLC to afford the compound **36** as a yellow solid (52 mg, 30% yield for two steps). UPLC−MS calculated for $C_{17}H_{15}N_4O_4$ $[M + H]^+$: 339.11, found 339.08.

Compound **36** (150 mg, 0.44 mmol) was suspended in thionyl chloride (0.64 mL, 8.8 mmol), and two drops of dry DMF were added. The mixture was stirred at reflux for 2 h. Excess thionyl chloride was removed in vacuo, and the resulting solid was dried. The resulting acyl chloride was used without further purification. Dry THF (15 mL) was added to the acyl chloride. The mixture was cooled to 0 °C, and subsequently, methylamine hydrochloride (45 mg, 0.67 mmol) was added. After stirring at room temperature for 2 h, the mixture was evaporated and purified by preparative HPLC to get 61.8 mg of compound **28** with a yield of 40%. ESI-MS calculated for $C_{18}H_{17}N_5O_3$ $[M + H]^+$ = 52.13. Obtained: 352.17. ^{1}H NMR (400 MHz, MeOD-d_4) δ 9.55 (s, 1H), 8.03 (s, 1H), 7.54 (s, 1H), 3.96 (s, 3H), 2.35 (s, 3H), 2.18 (s, 3H), 1.31 (t, J = 7.3 Hz, 3H). UPLC analysis (10 min from 10% to 100% (MeCN/H_2O containing 0.1% CF_3CO_2H)): retention time, 2.70 min; peak area, 98.12%.

Determination of Biochemical Binding Affinities to BET Proteins. Binding affinities of BET inhibitors to BRD2 (BD1 and BD2 proteins), BRD3 (BD1 and BD2 proteins), BRD4 (BD1 and BD2 proteins) were determined using our established fluorescence-polarization binding assays as described previously.[27]

Cell Growth Inhibition, Apoptosis Analysis, and Western Blotting. The human acute leukemia RS4;11 cell line (CRL-1873) was purchased from the American Type Culture Collection, and the human acute leukemia MOLM-13 cell line was purchased from the DSMZ German cell bank (ACC554). In all experiments, RS4;11 and MOLM-13 human leukemia cells were used within three months of thawing fresh vials. RS4;11 and MOLM-13 cells were cultured in RPMI 1640 media supplemented with 10% FBS and 1% penicillin−streptomycin at 37 °C in a humidified atmosphere containing 5% CO_2 in air.

In cell growth experiments, cells were seeded in 96-well cell culture plates at a density of 10000−20000 cells/well in 100 μL of culture medium. Each compound tested was serially diluted in the appropriate medium, and 100 μL of the diluted solution containing the tested compound was added to the appropriate wells of the cell plate. After addition of the tested compound, the cells were incubated for 4 days at 37 °C in an atmosphere of 5% CO_2. Cell growth was evaluated by a lactate dehydrogenase-based WST-8 assay (Dojindo Molecular Technologies) using a Tecan Infinite M1000 multimode microplate reader (Tecan, Morrisville, NC). The WST-8 reagent was added to the plate, incubated for at least 1 h, and read at 450 nm. The readings were normalized to the DMSO-treated cells, and the IC_{50} was calculated by nonlinear regression analysis using GraphPad Prism 6 software.

Flow cytometry was used to analyze effects of the drugs on cell cycle (propidium iodide staining) and apoptosis (annexin V and propidium iodide staining). Cell were treated with compounds at the indicated concentrations for 24 h, collected, stained, and analyzed by flow cytometry.

For Western blot analysis, 2 × 10^6 cells/well were treated with compounds at the indicated concentrations for various times. Cells were collected and lysed in RIPA buffer containing protease inhibitors. An amount of 20 μg of lysate was run in each lane of a PAGE−SDS and blotted into PVDF membranes. Antibodies for immunoblotting were BRD2, BRD3, and BRD4 purchased from Bethyl Laboratories (Montgomery, TX, USA), c-Myc from Cell Signaling Technology (Danvers, MA, USA), and GAPDH from Santa Cruz Biotechnologies (Dallas, TX, USA).

Efficacy and Pharmacodynamics Studies in the RS4;11 Xenograft Model in Mice. All animal experiments were done under the guidelines of the University of Michigan Committee for Use and Care of Animals and using an approved animal protocol (PRO00005315, PI, Shaomeng Wang).

To develop xenograft tumors, 5 × 10^6 RS4;11 cells with 50% Matrigel were injected subcutaneously on the dorsal side of severe combined immunodeficient (SCID) mice, obtained from Charles River, one tumor per mouse. When tumors reached ∼100 mm^3, mice were randomly assigned to treatment and vehicle control groups. Animals were monitored daily for any signs of toxicity and weighed 2−3 times per week during the treatment and weighed at least weekly after the treatment ended. Tumor size was measured 2−3 times per week by electronic calipers during the treatment period and at least weekly after the treatment was ended. Tumor volume was calculated as $V = LW^2/2$, where L is the length and W is the width of the tumor.

For pharmacodynamic analysis, resected RS4;11 xenograft tumor tissues were ground into powder in liquid nitrogen and lysed in lysis buffer (1% CHAPS, 150 mM NaCl, 20 mM Tris-HCl, 1 mM. EDTA, 1 mM EGTA, and COMPLETE proteinase inhibitor (Roche)). Whole tumor lysates were separated on 4−20% Novex gels. The separated proteins were transferred to a polyvinylidene difluoride membrane for immunoblotting. The following antibodies were used: rabbit polyclonal antibodies for BRD2 (A302-583A), BRD3 (A302-368A), and BRD4 (A301-985A100) from Bethyl Laboratories; c-Myc (D84C12), PARP (46D11), and caspase-3 (8G10) from Cell Signaling Technology, and actin goat polyclonal antibody from Santa Cruz Biotechnology. The secondary antibody used was horseradish peroxidase conjugated goat anti-rabbit (Thermo Scientific). The BIO-RAD Clarity Western Enhanced Chemiluminescence Substrates and HyBlot Chemiluminescence film were used for signal development and detection using a SRX-101A tabletop processor (Konica Minolta).

Determination of Drug Concentrations in Plasma and RS4;11 Tumor Tissue. Pharmacokinetics of compound **23** was determined in female SCID C.B-17 mice bearing RS4;11 tumors following a single intravenous dose of 5 mg/kg. Compound **23** was dissolved in the vehicle containing 20% (v/v) polyethylene glycol 400, 6% (v/v) Cremophor EL and 74% (v/v) PBS (20% PCP). Mice were sacrificed at 1, 3, 6, and 24 h after drug treatment and at 6 h after vehicle treatment, followed by collection of blood samples (300 μL) and tumor samples. Blood samples were centrifuged at 15 000 rpm for 10 min, then the supernatant plasma was saved for analysis. Isolated tumor samples were immediately frozen and ground with a mortar and pestle in liquid nitrogen. All plasma and tumor samples were stored at −80 °C prior to analysis.

Plasma and tumor concentrations of compound **23** were determined by a LC−MS/MS method developed and validated for this study. The LC−MS/MS method, consisting of a Shimadzu HPLC system and chromatographic separation of tested compound, was achieved using a Waters XBridge-C18 column (5 cm × 2.1 mm, 3.5 μm). An AB Sciex QTrap 5500 mass spectrometer equipped with an electrospray ionization source (Applied Biosystems, Toronto, Canada) in the positive-ion multiple reaction monitoring (MRM) mode was used for detection. The mobile phases were 0.1% formic acid in purified water (A) and 0.1% formic acid in acetonitrile (B). The

DOI: 10.1021/acs.jmedchem.6b01816
J. Med. Chem. 2018, 61, 462−481

gradient (B) was held at 10% (0−0.3 min), increased to 95% at 0.7 min, then held at isocratic 95% B for 2.3 min and then immediately stepped back down to 10% for 2 min re-equilibration. The flow rate was set at 0.4 mL/min.

In Vitro Metabolite Identification in Mouse Liver Microsomes. Compound **23** (10 μM) was incubated with mouse liver microsomes (MLM) and β-NADPH at 37 °C for 20 and 40 min. The reaction was quenched by adding a 3-fold volume of ice-cold acetonitrile. The mixture was centrifuged at 15 000 rpm for 10 min, and the supernatant was saved under −80 °C for analysis. The negative control samples were prepared by a similar procedure without NADPH or using boiled microsomes. The general approach for metabolite identification using AB Sciex QTrap 5500 mass spectrometer involves the following steps: (1) Obtain a product ion spectrum of the parent compound to establish fragmentation. (2) Interpret the spectrum to identify major fragment ion and possible neutral loss. (3) Collect spectra of samples using both established precursor ion scan and neutral loss scan. EMS scan of both control and samples were acquired also. (4) Run product ion scans and MRM scans for all possible metabolite identified from step 3 plus expected metabolite. (5) Interpret the spectrum of the metabolites and determine the structure with their logical fragmentation pattern.

■ ASSOCIATED CONTENT

Supporting Information

The Supporting Information is available free of charge on the ACS Publications website at DOI: 10.1021/acs.jmedchem.6b01816.

Western Blotting analysis of BRD2, BRD3, and BRD4 proteins in RS4;11 cells treated with compounds **8**, **23**, and **26**; ^{1}H NMR spectrum for compound **23**; ^{13}C NMR spectrum for compound **23**; UPLC−MS results for compound **23** PDF)

Coordinates information for structure representation (PDB)

Molecular formula strings and some data (CSV)

■ AUTHOR INFORMATION

Corresponding Author

*Phone: 1-734-615-0362. Fax: 1-734-647-9647. E-mail: shaomeng@umich.edu.

ORCID

Bing Zhou: 0000-0003-1813-8035

Shaomeng Wang: 0000-0002-8782-6950

Author Contributions

$^{\nabla}$B.Z., J.H., F.X., Z.C., L.B., E.F.-S., and M.L. contributed equally.

Notes

The authors declare the following competing financial interest(s): S. Wang, B. Zhou, F. Xu, J. Hu, L. Bai, C.-Y. Yang, D. McEachern, and S. Przybranowski are co-inventors for BET degraders disclosed in this study. The University of Michigan has filed a number of patent applications related to these BET degraders, which have been licensed to Medsyn Biopharma. S. Wang is a co-founder, stock holder, and consultant for Medsyn Biopharma.

■ ACKNOWLEDGMENTS

This study is supported in part by funding from the Breast Cancer Research Foundation (to S.W.), the University of Michigan Comprehensive Cancer Center Strategic Fund for Breast Cancer (to S.W.), the University of Michigan Comprehensive Cancer Center Core Grant from the National Cancer Institute, NIH (Grant P30CA046592), and Medsyn Biopharma.

■ ABBREVIATIONS USED

AML, acute myeloid leukemia; BD1, bromodomain 1; BD2, bromodomain 2; BET, bromodomain and extra-terminal domain; BINAP, 2,2′-bis(diphenylphosphino)-1,1′-binaphthalene; BRD2, bromodomain-containing protein 2; BRD3, bromodomain-containing protein 3; BRD4, bromodomain-containing protein 4; BRDT, bromodomain testis-specific protein; FP, fluorescence polarization; GAPDH, glyceraldehyde 3-phosphate dehydrogenase; MLL1, mixed lineage leukemia protein 1; MRM, multiple reaction monitoring; NUT, nuclear protein in testis; PBS, phosphate buffered saline; PD, pharmacodynamics; PK, pharmacokinetics; PROTAC, proteolysis targeting chimera

■ REFERENCES

(1) Patel, D. J.; Wang, Z. Readout of epigenetic modifications. *Annu. Rev. Biochem.* **2013**, *82*, 81−118.

(2) Belkina, A. C.; Denis, G. V. BET domain co-regulators in obesity, inflammation and cancer. *Nat. Rev. Cancer* **2012**, *12*, 465−477.

(3) Dawson, M. A.; Kouzarides, T.; Huntly, B. J. P. Targeting epigenetic readers in cancer. *N. Engl. J. Med.* **2012**, *367*, 647−657.

(4) Arrowsmith, C. H.; Bountra, C.; Fish, P. V.; Lee, K.; Schapira, M. Epigenetic protein families: a new frontier for drug discovery. *Nat. Rev. Drug Discovery* **2012**, *11*, 384−400.

(5) Muller, S.; Filippakopoulos, P.; Knapp, S. Bromodomains as therapeutic targets. *Expert Rev. Mol. Med.* **2011**, *13*, e29.

(6) Chung, C.-W. Small molecule bromodomain Inhibitors: extending the druggable genome. *Prog. Med. Chem.* **2012**, *51*, 1−55.

(7) Filippakopoulos, P.; Qi, J.; Picaud, S.; Shen, Y.; Smith, W. B.; Fedorov, O.; Morse, E. M.; Keates, T.; Hickman, T. T.; Felletar, I.; Philpott, M.; Munro, S.; McKeown, M. R.; Wang, Y.; Christie, A. L.; West, N.; Cameron, M. J.; Schwartz, B.; Heightman, T. D.; La Thangue, N.; French, C. A.; Wiest, O.; Kung, A. L.; Knapp, S.; Bradner, J. E. Selective inhibition of BET bromodomains. *Nature* **2010**, *468*, 1067−1073.

(8) Boi, M.; Gaudio, E.; Bonetti, P.; Kwee, I.; Bernasconi, E.; Tarantelli, C.; Rinaldi, A.; Testoni, M.; Cascione, L.; Ponzoni, M.; Mensah, A. A.; Stathis, A.; Stussi, G.; Riveiro, M. E.; Herait, P.; Inghirami, G.; Cvitkovic, E.; Zucca, E.; Bertoni, F. The BET bromodomain inhibitor OTX015 affects pathogenetic pathways in preclinical B-cell tumor models and synergizes with targeted drugs. *Clin. Cancer Res.* **2015**, *21*, 1628−1638.

(9) Berthon, C.; Raffoux, E.; Thomas, X.; Vey, N.; Gomez-Roca, C.; Yee, K.; Taussig, D. C.; Rezai, K.; Roumier, C.; Herait, P.; Kahatt, C.; Quesnel, B.; Michallet, M.; Recher, C.; Lokiec, F.; Preudhomme, C.; Dombret, H. Bromodomain inhibitor OTX015 in patients with acute leukaemia: a dose-escalation, phase 1 study. *Lancet Haematol.* **2016**, *3*, 186−195.

(10) Odore, E.; Lokiec, F.; Cvitkovic, E.; Bekradda, M.; Herait, P.; Bourdel, F.; Kahatt, C.; Raffoux, E.; Stathis, A.; Thieblemont, C.; Quesnel, B.; Cunningham, D.; Riveiro, M. E.; Rezaï, K. Phase I population pharmacokinetic assessment of the oral bromodomain Inhibitor OTX015 in patients with haematologic malignancies. *Clin. Pharmacokinet.* **2016**, *55*, 397−405.

(11) Coudé, M.-M.; Braun, T.; Berrou, J.; Dupont, M.; Bertrand, S.; Masse, A.; Raffoux, E.; Itzykson, R.; Delord, M.; Riveiro, M. E.; Herait, P.; Baruchel, A.; Dombret, H.; Gardin, C. BET inhibitor OTX015 targets BRD2 and BRD4 and decreases c-MYC in acute leukemia cells. *Oncotarget* **2015**, *6*, 17698−17712.

(12) Nicodeme, E.; Jeffrey, K. L.; Schaefer, U.; Beinke, S.; Dewell, S.; Chung, C. W.; Chandwani, R.; Marazzi, I.; Wilson, P.; Coste, H.; White, J.; Kirilovsky, J.; Rice, C. M.; Lora, J. M.; Prinjha, R. K.; Lee, K.; Tarakhovsky, A. Suppression of inflammation by a synthetic histone mimic. *Nature* **2010**, *468*, 1119−1123.

(13) Mirguet, O.; Gosmini, R.; Toum, J.; Clement, C. A.; Barnathan, M.; Brusq, J. M.; Mordaunt, J. E.; Grimes, R. M.; Crowe, M.; Pineau, O.; Ajakane, M.; Daugan, A.; Jeffrey, P.; Cutler, L.; Haynes, A. C.; Smithers, N. N.; Chung, C. W.; Bamborough, P.; Uings, I. J.; Lewis, A.; Witherington, J.; Parr, N.; Prinjha, R. K.; Nicodeme, E. Discovery of epigenetic regulator I-BET762: lead optimization to afford a clinical candidate inhibitor of the BET bromodomains. *J. Med. Chem.* **2013**, *56*, 7501−7515.
(14) Stathis, A.; Zucca, E.; Bekradda, M.; Gomez-Roca, C.; Delord, J. P.; de La Motte Rouge, T.; Uro-Coste, E.; de Braud, F.; Pelosi, G.; French, C. A. Clinical response of carcinomas harboring the BRD4-NUT oncoprotein to the targeted bromodomain inhibitor OTX015/MK-8628. *Cancer Discovery* **2016**, *6*, 492−500.
(15) Chaidos, A.; Caputo, V.; Gouvedenou, K.; Liu, B.; Marigo, I.; Chaudhry, M. S.; Rotolo, A.; Tough, D. F.; Smithers, N. N.; Bassil, A. K.; Chapman, T. D.; Harker, N. R.; Barbash, O.; Tummino, P.; Al-Mahdi, N.; Haynes, A. C.; Cutler, L.; Le, B.; Rahemtulla, A.; Roberts, I.; Kleijnen, M.; Witherington, J. J.; Parr, N. J.; Prinjha, R. K.; Karadimitris, A. Potent antimyeloma activity of the novel bromodomain inhibitors I-BET151 and I-BET762. *Blood* **2014**, *123*, 697−705.
(16) Banerjee, C.; Archin, N.; Michaels, D.; Belkina, A. C.; Denis, G. V.; Bradner, J.; Sebastiani, P.; Margolis, D. M.; Montano, M. BET bromodomain inhibition as a novel strategy for reactivation of HIV-1. *J. Leukocyte Biol.* **2012**, *92*, 1147−1154.
(17) Zhu, J.; Gaiha, G. D.; John, S. P.; Pertel, T.; Chin, C. R.; Gao, G.; Qu, H.; Walker, B. D.; Elledge, S. J.; Brass, A. L. Reactivation of latent HIV-1 by inhibition of BRD4. *Cell Rep.* **2012**, *2*, 807−816.
(18) Denis, G. V. Bromodomain coactivators in cancer, obesity, type 2 diabetes, and inflammation. *Discovery Med.* **2010**, *10*, 489−499.
(19) Matzuk, M. M.; McKeown, M. R.; Filippakopoulos, P.; Li, Q.; Ma, L.; Agno, J. E.; Lemieux, M. E.; Picaud, S.; Yu, R. N.; Qi, J.; Knapp, S.; Bradner, J. E. Small-molecule inhibition of BRDT for male contraception. *Cell* **2012**, *150*, 673−684.
(20) Sakamoto, K. M.; Kim, K. B.; Kumagai, A.; Mercurio, F.; Crews, C. M.; Deshaies, R. J. Protacs: Chimeric molecules that target proteins to the Skp1−Cullin−F box complex for ubiquitination and degradation. *Proc. Natl. Acad. Sci. U. S. A.* **2001**, *98*, 8554−8559.
(21) Toure, M.; Crews, C. M. Small-molecule PROTACS: new approaches to protein degradation. *Angew. Chem., Int. Ed.* **2016**, *55*, 1966−1973.
(22) Bondeson, D. P.; Mares, A.; Smith, I. E. D.; Ko, E.; Campos, S.; Miah, A. H.; Mulholland, K. E.; Routly, N.; Buckley, D. L.; Gustafson, J. L.; Zinn, N.; Grandi, P.; Shimamura, S.; Bergamini, G.; Faelth-Savitski, M.; Bantscheff, M.; Cox, C.; Gordon, D. A.; Willard, R. R.; Flanagan, J. J.; Casillas, L. N.; Votta, B. J.; den Besten, W.; Famm, K.; Kruidenier, L.; Carter, P. S.; Harling, J. D.; Churcher, I.; Crews, C. M. Catalytic in vivo protein knockdown by small-molecule PROTACs. *Nat. Chem. Biol.* **2015**, *11*, 611−617.
(23) Winter, G. E.; Buckley, D. L.; Paulk, J.; Roberts, J. M.; Souza, A.; Dhe-Paganon, S.; Bradner, J. E. Phthalimide conjugation as a strategy for in vivo target protein degradation. *Science* **2015**, *348*, 1376−1381.
(24) Raina, K.; Lu, J.; Qian, Y.; Altieri, M.; Gordon, D.; Rossi, A. M. K.; Wang, J.; Chen, X.; Dong, H.; Siu, K.; Winkler, J. D.; Crew, A. P.; Crews, C. M.; Coleman, K. G. PROTAC-induced BET protein degradation as a therapy for castration-resistant prostate cancer. *Proc. Natl. Acad. Sci. U. S. A.* **2016**, *113*, 7124−7129.
(25) Lu, J.; Qian, Y.; Altieri, M.; Dong, H.; Wang, J.; Raina, K.; Hines, J.; Winkler, J. D.; Crew, A. P.; Coleman, K.; Crews, C. M. Hijacking the E3 ubiquitin ligase cereblon to efficiently target BRD4. *Chem. Biol.* **2015**, *22*, 755−763.
(26) Zengerle, M.; Chan, K. H.; Ciulli, A. Selective small molecule induced degradation of the BET bromodomain protein BRD4. *ACS Chem. Biol.* **2015**, *10*, 1770−1777.
(27) Ran, X.; Zhao, Y.; Liu, L.; Bai, L.; Yang, C.-Y.; Zhou, B.; Meagher, J. L.; Chinnaswamy, K.; Stuckey, J. A.; Wang, S. Structure-based design of γ-carboline analogues as potent and specific BET bromodomain inhibitors. *J. Med. Chem.* **2015**, *58*, 4927−4939.
(28) Zeldis, J. B.; Knight, R.; Hussein, M.; Chopra, R.; Muller, G. A review of the history, properties, and use of the immunomodulatory compound lenalidomide. *Ann. N. Y. Acad. Sci.* **2011**, *1222*, 76−82.
(29) Fischer, E. S.; Bohm, K.; Lydeard, J. R.; Yang, H.; Stadler, M. B.; Cavadini, S.; Nagel, J.; Serluca, F.; Acker, V.; Lingaraju, G. M.; Tichkule, R. B.; Schebesta, M.; Forrester, W. C.; Schirle, M.; Hassiepen, U.; Ottl, J.; Hild, M.; Beckwith, R. E. J.; Harper, J. W.; Jenkins, J. L.; Thoma, N. H. Structure of the DDB1-CRBN E3 ubiquitin ligase in complex with thalidomide. *Nature* **2014**, *512*, 49−53.
(30) Delmore, J. E.; Issa, G. C.; Lemieux, M. E.; Rahl, P. B.; Shi, J.; Jacobs, H. M.; Kastritis, E.; Gilpatrick, T.; Paranal, R. M.; Qi, J.; Chesi, M.; Schinzel, A. C.; McKeown, M. R.; Heffernan, T. P.; Vakoc, C. R.; Bergsagel, P. L.; Ghobrial, I. M.; Richardson, P. G.; Young, R. A.; Hahn, W. C.; Anderson, K. C.; Kung, A. L.; Bradner, J. E.; Mitsiades, C. S. BET bromodomain inhibition as a therapeutic strategy to target c-Myc. *Cell* **2011**, *146*, 904−917.
(31) Wang, S.; Ran, X.; Zhao, Y.; Yang, C.-Y.; Liu, L.; Bai, L.; McEachern, D.; Stuckey, J.; Meagher, J. L.; Sun, D.; Li, X.; Zhou, B.; Karatas, H.; Luo, R.; Chinnaiyan, A.; Asangani, I. A. Preparation of pyridoindole, pyridazinoindole and pyrimidinoindole compounds as BET bromodomain inhibitors. US 20140256706 A1, September 11, 2014.
(32) Bai, L.; Zhou, B.; Yang, C.-Y.; Ji, J.; McEachern, D.; Przybranowski, S.; Jiang, H.; Hu, J.; Xu, F.; Zhao, Y.; Liu, L.; Fernandez-Salas, E.; Xu, J.; Dou, Y.; Wen, B.; Sun, D.; Meagher, J. L.; Stuckey, J.; Hayes, D. F.; Li, S.; Ellis, M. J.; Wang, S. Targeted degradation of BET proteins in triple-negative breast cancer. *Cancer Res.* **2017**, DOI: 10.1158/0008-5472.CAN-16-2622.

DOI: 10.1021/acs.jmedchem.6b01816
J. Med. Chem. 2018, 61, 462−481